European Journal of Pharmaceutics and Biopharmaceutics 165 (2021) 319–336

Contents lists available at ScienceDirect

European Journal of Pharmaceutics and Biopharmaceutics

journal homepage: www.elsevier.com/locate/ejpb

Application of ultraviolet, visible, and infrared light imaging in protein-based biopharmaceutical formulation characterization and development studies

Marieke E. Klijn [a,*], Jürgen Hubbuch [b]

[a] Department of Biotechnology, Delft University of Technology, Van der Maasweg 9, Delft 2629 HZ, the Netherlands
[b] Institute of Engineering in Life Sciences, Section IV: Biomolecular Separation Engineering, Karlsruhe Institute of Technology (KIT), Fritz-Haber-Weg 2, 76131 Karlsruhe, Germany

ARTICLE INFO

Keywords:
Image processing
Machine learning
Formulation development
Protein analytics
High-throughput screening
Computer vision

ABSTRACT

Imaging is increasingly more utilized as analytical technology in biopharmaceutical formulation research, with applications ranging from subvisible particle characterization to thermal stability screening and residual moisture analysis. This review offers a comprehensive overview of analytical imaging for scientists active in biopharmaceutical formulation research and development, where it presents the unique information provided by the ultraviolet (UV), visible (Vis), and infrared (IR) sections in the electromagnetic spectrum. The main body of this review consists of an outline of UV, Vis, and IR imaging techniques for several (bio)physical properties that are commonly determined during protein-based biopharmaceutical formulation characterization and development studies. The review concludes with a future perspective of applied imaging within the field of biopharmaceutical formulation research.

1. Introduction

Biopharmaceutical formulation characterization is an integral part of biopharmaceutical research and development, where insight is generated on the product's critical quality attributes as a function of formulation (processing) parameters, such as pH [1], excipients [2,3] or temperature [4]. This results from the Quality by Design (QbD) approach, which strives for a systematic development of biopharmaceutical products and their production processes based on predefined product quality characteristics [5]. Characterization studies are therefore essential to determine manufacturability as well as the safety and efficacy of biopharmaceutical products [6]. Some analytical techniques employed for characterization studies can also be applied as process analytical technology (PAT) to enable product quality monitoring during processing for (near)-real time release applications, thereby minimizing production and product quality risks [7]. Characterization studies utilize a wide range of analytical technologies to capture both biophysical protein properties, such as aggregation tendency [8] or thermal stability [9–11], and physical formulation properties, such as surface tension [12,13]. One of the analytical techniques applied for characterization studies is imaging, where an image is defined as a visual 2-D spatial representation of the subject. Imaging is able to capture a multitude of characteristics as the format of an image has been expanded beyond a digital visible light image by using the breadth of the electromagnetic spectrum. In addition to its broad information content, the non-invasive nature of imaging is beneficial during biopharmaceutical characterization and development studies, as well as for PAT purposes, as product interference can lead to unrepresentative results. These attributes make imaging a widely applicable analytical technique, but its full potential not yet reached for biopharmaceutical research and development studies as further optimization is needed, such as shorter acquisition times, (cost-competitive) multiplexed imaging equipment, and advanced data analytics. This review provides information to show the current role of analytical imaging and understand the role it will play in biopharmaceutical characterization and development studies upon realization of its full potential. This is done by presenting imaging techniques, the respective part of electromagnetic spectrum, an overview of current imaging possibilities, and the novel insight these applications have already generated.

A general imaging setup is schematically shown in Fig. 1 and consists of emission by a light source (a), detection by means of an image acquisition device (b), and a processor and control unit (c). An image

* Corresponding author.
E-mail address: m.e.klijn@tudelft.nl (M.E. Klijn).

https://doi.org/10.1016/j.ejpb.2021.05.013
Received 23 November 2020; Received in revised form 29 March 2021; Accepted 12 May 2021
Available online 27 May 2021

acquisition device is employed to capture different types of light-matter interaction effects (d), namely transmitance, absorption, reflectance, scattering, or fluorescence. A depiction of each of these effects is shown in Fig. 1 as well.

Transmittance refers to the degree of light passing through matter without any interaction. The term reflectance describes light beams that follow the law of reflection, where the incident photons are reflected under an equal angle, as well as diffuse reflection, where scattering of light occurs without photon energy absorption [14]. Absorbance describes the situation where a photon's energy is absorbed by the respective matter. This occurs when a photon carries an energy that is similar to a certain molecular transition. As a photon's energy is inversely proportional to its wavelength, different molecular transitions occur as a result of photon absorbance across the electromagnetic spectrum. An example of electron excitation [15] and vibrational transitions [16] is depicted in the Jablonski diagram in Fig. 1. Fluorescence occurs when an electron returns to its ground state from an excited electronic state induced by photon absorption. This return results in the emission of a photon with an energy equal to the energy difference between the excited and ground state [15,17]. The emitted photon carries a lower energy compared to the incident photon as some of the initially absorbed energy dissipates via non-radiative transitions, such as molecular relaxation [17].

The term scattering is used to define an event where incident photons interact with the respective matter and are subsequently emitted in different directions. This interaction results in an excitation to the so-called virtual state because the photon's energy is not resonant with a molecular transition and is rapidly ($<10^{-15}$ s) followed by the emission of a photon upon returning to the ground state [18,19]. The emitted photons' energy can remain similar (elastic scattering) or change (inelastic scattering) [19,20]. This is illustrated in the Jablonski diagram in Fig. 1, where elastic scattering shown by I and inelastic scattering is shown by II and III. The direction of elastic scattering is dependent on the size of the particle with respect to the wavelength of the incident photon. Rayleigh scattering occurs for particles with a size smaller than one-tenth of the wavelength, where the scattering is distributed in all directions. Forward scattering becomes dominant for particles larger than one-tenth of the photon's wavelength, where Mie scattering occurs for particles between one-tenth and 1 time the wavelength. Optical scattering occurs for particles larger than the wavelength of the incident photon. Inelastic scattering results in the emission of a photon carrying a lower or higher energy than the incident photon, which is referred to as Raman Stokes (II, Fig. 1) or anti-Stokes (III, Fig. 1) scattering, respectively [20]. Inelastic Raman scattering accounts only for approximately 1 in 10^{10} incident photons [19,21]. As most molecules are in their ground state at ambient temperature, mostly Raman Stokes scattering occurs [22]. More information on Raman scattering is provided in Section 2.4, where Raman scattering is discussed alongside infrared photon absorption.

The employed wavelength of the light source can vary within the

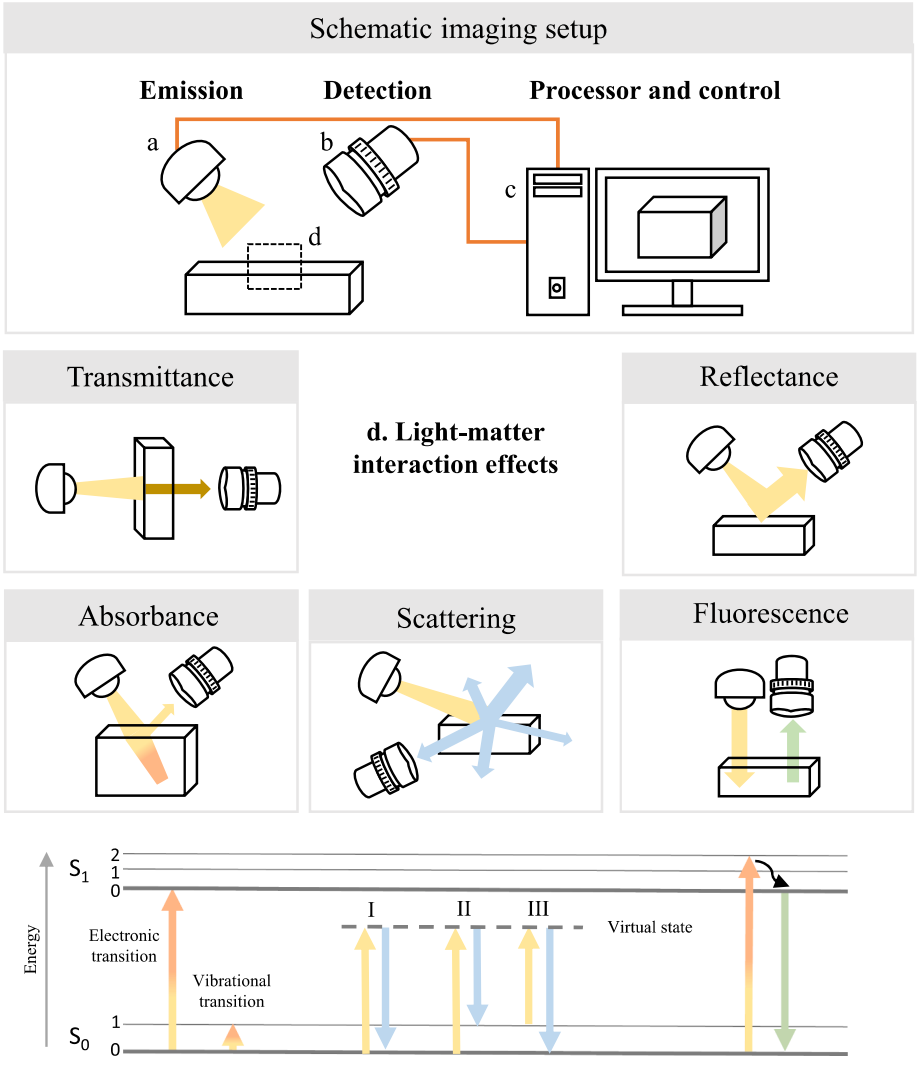

Fig. 1. A schematic of a general imaging setup, showing (a) emission by a light source, (b) detection by an image acquisition device, and (c) a processor and control unit, where orange lines indicate control and data transfer connections. The inset (d) refers to the five light-matter interaction effects employed for image acquisition, showing transmittance (brown), absorbance (red), reflectance (yellow), scattering (blue), and fluorescence (green) of an incoming light beam. A Jablonski diagram is shown below to illustrate the transitions for absorbance, scattering (I: Rayleigh scattering, II: Raman Stokes scattering, and III: Raman anti-Stokes scattering), and fluorescence. (For interpretation of the references to color in this figure legend, the reader is referred to the web version of this article.)

electromagnetic spectrum, of which a part is shown on the left side of Fig. 2. This review focuses on different regions of the electromagnetic spectrum ranging from ultraviolet (UV, 190 nm – 380 nm) to the far infrared (FIR, 30–1 mm) range, as these wavelengths cover the majority of imaging techniques relevant for protein-based biopharmaceutical characterization and development studies.

The first part of the review presents the relevant and unique information content of each region and is followed by a brief overview of required data analytical steps to extract and utilize the information content. The review continues with the application of the electromagnetic spectrum wavelength regions, sectioned per (bio)physical property of protein-based biopharmaceutical products and/or the formulation. The review concludes with a future perspective on imaging trends and optimizations in the field of biopharmaceutical characterization and development research.

2. Electromagnetic spectrum: Ultraviolet to far infrared (190–1 mm)

The UV to FIR (190–1 mm) range is a rich source of information, meaning the selection of a particular light source for an imaging technique depends on the desired (bio)physical property to extract or to represent. A general overview of the information content within the UV to FIR range is displayed on the right side in Fig. 2. The following subsections concisely present the depicted information content, ordered per region within the UV to FIR range.

2.1. Ultraviolet (190–380 nm)

The UV region can be employed for reflective and fluorescent imaging purposes [23]. Of these two, only fluorescent UV imaging will be introduced in this review, as this technique is applied for protein-based biopharmaceutical characterization studies to determine the presence or spatial location of proteins. Proteins can be located as a result of intrinsic fluorescence of the aromatic amino acid tryptophan, tyrosine, and phenylalanine. These specific amino acids absorb photons with a wavelength in the UV region, with a maximum absorbance around 280, 275, and 260 nm, respectively, and emit the residual energy at a maximum near 350, 300, and 280 nm, respectively [24]. Tryptophan plays a dominant role in UV imaging due to its emission wavelength and relatively high fluorescence quantum yield [25], where the fluorescence quantum yield determines the emission intensity. Fluorescence emission intensity can be strongly influenced by environmental factors, such as solution polarity or ionic strength [26] and resonance energy transfer to neighboring residues [27]. In addition to intrinsic protein fluorescence, extrinsic protein fluorescence is also applied for fluorescent imaging. Extrinsic fluorescence is achieved by adding fluorescent dyes that (non) covalently bind to protein molecules [28]. This procedure facilitates fluorescent imaging independent of the presence of aromatic amino acids and for a wider range of wavelengths (also outside the UV range) to enhance detection specificity.

2.2. Visible light (380-750 nm)

Visible light imaging is commonly used for the identification of objects and texture by means of reflectance, transmittance, and absorbance. Reflectance and transmittance imaging allow for the identification of objects, where reflectance provides information on the surface of the sample and transmittance provides surface and subsurface information [29]. Visible light imaging is also employed for the documentation of colors. Colors are commonly utilized to identify texture by evaluating the spatial distribution of color or shade levels, where texture is defined as a local variation that is too small to qualify as an object [30]. Object identification by means of transmittance is based on light obstruction, but this mode can also encounter uncontrollable obscuration of the light path, which may block transmittance entirely. Thus, for transmittance imaging sample transparency needs to be considered.

Contrast enhancement expands the information content of visible light images towards the type of matter that is captured as an object or texture. Commonly used methods are light polarization, dark-field

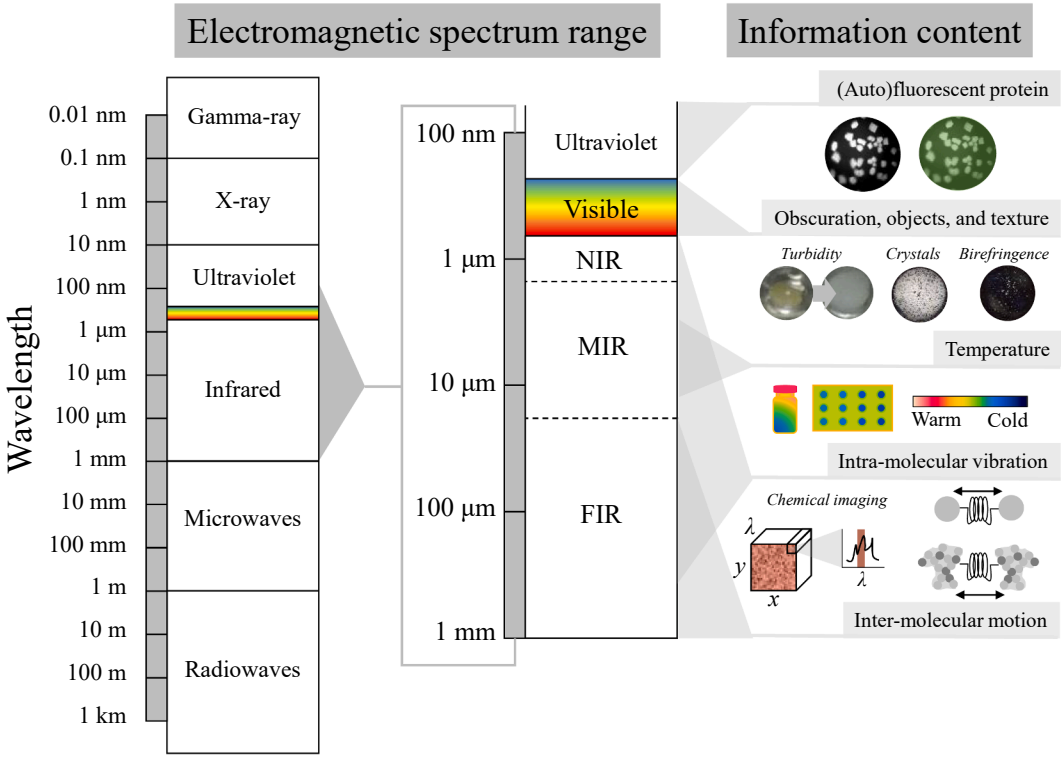

Fig. 2. Overview of the electromagnetic spectrum range discussed in this review (left) and a general indication of the corresponding information content (right).

illumination, phase contrast imaging, or differential interference contrast imaging, where additional hardware components are added or the hardware configuration is adjusted [31]. For example, light polarization involves the implementation of a filter to obtain a light wave oscillation in a particular direction, which can be a single direction, a rotational direction, or under an angle, such as used for cross-polarization [32]. Polarized light can be used to distinguish between isotropic and anisotropic materials, such as crystals, because anisotropic material influences the direction of polarized light (birefringence) [33] and isotropic material does not. Dark-field illumination is an example of altering the angle between the light source and the image acquisition device to solely capture light that is reflected if objects interfere [34]. Such a change in configuration can be applied to obtain an improved detection of colorless or transparent objects.

2.3. Thermal radiation (8–14 μm)

Thermal radiation spans multiple electromagnetic spectrum regions and is defined as radiant energy that is solely due to the object's temperature [35]. The detection of temperature is of interest for protein-based biopharmaceutical characterization and development studies, as temperature is an environmental factor that influences proteins' colloidal, conformational, and chemical stability [36]. Monitoring temperature via imaging is called thermography and it captures the rate with which thermal radiation leaves an object, where lower temperatures result in longer wavelengths emitted with a lower intensity, and vice versa. This makes thermography notably different from other imaging techniques as thermography does not require a light source. Thus, a schematic image acquisition setup, such as depicted in Fig. 1, would be without an external emission source. Capturing the temperature of an object is sensitive to a multitude of object and environmental factors. Among the most relevant factors are the object's surface area and emissivity (the degree of radiation of the material) as well as properties of the atmosphere, the temperature of surrounding material, and the angle and distance between the camera and the captured surface [37]. These dependencies result in the need for both object and surrounding characterization, as well as device calibration to obtain reliable output for analysis [37,38]. Three subsections in the infrared region are often used for thermography, namely 0.9 – 1.7 μm, 3 – 5 μm, and 8 – 14 μm, which are called the short-wave (SW), mid-wave (MW), and long-wave (LW) region, respectively. The LW region is considered most applicable for biopharmaceutical characterization purposes, as objects with relevant temperatures (approximately from −80 °C to 100 °C) emit most of the thermal radiation in this range and LW detection hardware is relatively inexpensive while providing sufficient thermal sensitivity (order of magnitude of 0.05 °C) [38]. Nevertheless, MW-based thermography can also be applied for biopharmaceutical characterization purposes, where it may overcome issues with resolution, temperature contrast, and reflection that may be encountered with LW-based thermography [38].

2.4. Near- and mid-infrared (750–10 μm)

As depicted in Fig. 2, the near- and mid-infrared region (NIR at 750 nm to 2.5 μm and MIR at 2.5 μm to 30 μm, respectively) can be used to extract information on intramolecular vibrations via absorption or scattering profiles. Imaging in the MIR and NIR region obtains similar fundamental information as IR spectroscopic techniques, but in contrast to spectroscopy, imaging gathers multiple spectra in the spatial dimension instead of a single spectrum per sample. It is often referred to as chemical imaging, vibrational imaging, infrared imaging, or hyperspectral imaging. The actual images are obtained by selecting one or multiple parts of the spectrum for visualization in the spatial dimension of the sample, as schematically depicted in Fig. 2 under the corresponding section. For protein-based biopharmaceutical characterization studies, NIR and MIR absorbance spectra are of interest as particular parts of the spectra have been empirically correlated to structural protein properties, such as secondary structural motifs [39–42]. In turn, the type and amount of structural protein properties allow for a distinction between different proteins as well as structural changes of a protein.

Photon absorption in the NIR and MIR region of the electromagnetic region leads to vibrational transition, where energy is absorbed if the photon energy is equal to the difference in a vibrational state [16]. However, the key selection rule for IR absorption states that a photon will only be absorbed if the electric dipole moment of the molecule changes as a result of the vibrational motion [22]. This means that IR absorbance occurs for polar bonds and nonsymmetric vibrations. Absorbance in the MIR region generates information on atomic stretching and bending of fundamental vibrations (transition from the ground state to the first excited vibrational state), while absorbance in the NIR region provides information on overtone bonds (transition from the ground state to a second or third state) and combination bonds (vibration interactions of fundamental bonds). NIR absorbance spectra are often obtained by means of transmittance or (trans)reflectance detection modes [43,44] and absorption in the MIR region is obtained by means of the attenuated total reflectance (ATR) mode, because strong absorption is a limiting factor for MIR. The ATR mode uses a highly reflective element, which fully reflects the incident beam, resulting in an evanescent wave that interacts with the sample on top of the ATR element. The evanescent wave only interacts with a thin layer of the sample, thereby preventing absorption saturation [44]. Because of the different wavelength regions, MIR and NIR measurements have different strengths and weaknesses. A disadvantage of NIR is that the absorption bonds are 10–100 times weaker than the corresponding MIR bonds [44] and show largely overlapping absorption curves, which complicates band assignment and data interpretation. However, the low absorption coefficient in the NIR region can be also an advantage, as it allows for a higher penetration depth than MIR, which is desirable for thicker samples [45], solids [44], and measurements through glass [19]. Both MIR and NIR have the disadvantage that water bonds absorb strongly, as it is a polar molecule, and in the same range as protein-related bonds. MIR shows the strongest water bond absorption and is therefore most adversely affected by the dominant water signal [39,44].

In addition to absorbance, the NIR region is also used to capture inelastic Raman scattering. As mentioned in the Introduction, Raman scattering occurs when the incident photons interact with matter and scatter after exchange of energy. The selection rule that applies to Raman scattering is the change in polarizability of the molecule as a result of the vibrational motions and the energy that is exchanged is equal to the energy needed for the respective vibrational transition [19]. Thus, similar to NIR/MIR absorption, a change in vibrational state is the cause of the energy difference between the incident and scattered photon. However, Raman scattering is fundamentally different as it is a scattering event and only occurs if there is a change in molecular polarizability instead of the electric dipole moment for NIR/MIR photon absorption [22]. Due to this fundamental difference, Raman scattering occurs for symmetric stretching vibrations and results in the inefficient Raman scattering of polar molecules, such as water [44,46]. This means a relatively weak signal of water is obtained in a Raman spectrum, compared to NIR and MIR absorption [47]. Raman scattering is regarded as an alternative as well as a complementary source of property information next to MIR and NIR absorbance because it provides structural information and has the ability to detect IR inactive bonds.

Raman scattering occurs at a range of wavelengths, but several compounds fluoresce when illuminated with photons of short wavelengths and the subsequent fluorescence intensity often overpowers the Raman signal [19]. Using excitation at 785, 830, and 1064 nm (NIR region), the wavelengths are long enough to minimize such fluorescence effects. However, longer wavelengths for excitation decrease the efficiency of Raman scattering as scattering intensity is inversely proportional to the fourth power of the wavelength [16]. Another approach to minimize fluorescence is the use of pulsed excitation where one can

benefit from the different time scales of fluorescence or Raman scattering events [47]. The fundamental difference between these phenomena results in a different emission timescale, namely 10^{-8}–10^{-9} s for fluorescence compared to $< 10^{-15}$ s for scattering [18]).

2.5. Far infrared (30 μm-1 mm)

Absorbance in the far-infrared (FIR) region of the electromagnetic spectrum is used for chemical imaging in a similar fashion as mentioned in the previous section on NIR and MIR. The so-called terahertz (THz) region is often applied, which approximately ranges from 10 μm to 1 mm (0.3–30 THz). The wavelength in the FIR region is longer compared to NIR and MIR, which causes the incident photons to have a lower energy. The light in this region is therefore predominantly influenced by intermolecular motions or crystalline lattice vibrations [48]. Spectroscopic applications using the FIR region are able to distinguish between different protein quaternary structures and higher-order structures, as well the hydration level in proteins [48,49]. Imaging in the FIR region has advantages over the other IR imaging approaches, as FIR light can penetrate samples up to 3 mm [48], meaning it allows one to obtain spectral data from within the sample, without destroying the sample.

3. Image processing and analysis

Once an image is captured by the acquisition device, the raw data requires further processing before the information content can be analyzed and interpreted. Depending on the application, several steps are involved during image processing and analysis, namely pre-processing, segmentation, description, and interpretation [50]. These steps are schematically depicted in Fig. 3.

Pre-processing of data is used to improve data quality and prepare extraction of information, such as noise reduction or contrast enhancement. The improved image is further processed by means of segmentation. Segmentation aims to obtain solely the information that is of interest for the respective application. This can entail spatial segmentation, by extracting information from a part of the image (left icon in Fig. 3 at the Segmentation section), or by characteristic segmentation, such as the extraction of a specific color level (right icon in Fig. 3 at the Segmentation section). The segmented information is passed on to the description step. Here, imaging-based features are extracted that quantify the information in the image. For example, this involves information extraction on lines, objects, or texture. Quantification is done by extracting, for instance, pixel counts, pixel intensity, color levels, or a change in any of these properties over time or in their spatial dimensions. The final step, interpretation, uses the extracted features to fulfill the set-out task. To illustrate the last step, the schematic overview in Fig. 3 shows the identification of objects and the ratio between certain colored objects. The conversion of the imaging-based features to interpretable results is often supported by multivariate data analysis and (un) supervised machine learning approaches. An extensive overview of multivariate image analysis for both spectral and visible light images is provided by Prats-Montalban et al. [51].

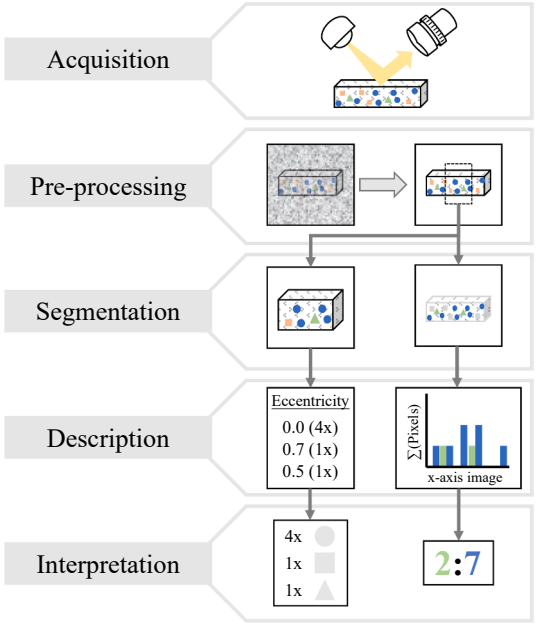

Fig. 3. Schematic overview of general steps performed during image processing and image analysis.

4. Imaging applications

The following sections cover how imaging with different parts of the electromagnetic spectrum is currently utilized for protein-based biopharmaceutical formulation characterization and development studies, sectioned per (bio)physical property. This review covers (bio)physical properties that are captured by means of imaging and that are applied for the most common protein-based biopharmaceutical formulation formats, namely liquid, freeze-dried, and spray-dried formulations. An overview of the content of this review is listed in Table 1. Table 1 includes the applications, the employed imaging methods, the corresponding electromagnetic spectrum, as well as the main information that is obtained with each method.

4.1. Subvisible particle characterization

Particles are defined as a minute piece of matter with defined physical boundaries [145] and can be divided into four quantitative size-based categories, namely > 100 μm, 1–100 μm, 0.1–1 μm (submicron particles), and < 100 nm (nanoparticles) [146]. The first category is often referred to as visible particles, while the latter 3 categories are often referred to as subvisible particles, which spans from protein monomers to soluble and insoluble protein aggregates. Particle formation in protein-based biopharmaceutical products is, on the one hand, an undesired phenomenon, as inherent drug product-related particles such as protein aggregates can cause adverse immune responses [147] and intrinsic or extrinsic particles, such as silicone droplets or lint, may induce proteinaceous particle formation [148,149]. On the other hand, particle formation can also be a goal of processing and formulation, for example when developing a crystalline or dry powder product. In the following subsections, imaging-based analytics for subvisible particle detection and characterization in liquid and solid formulations will be covered. Imaging-based techniques for visible particle characterization are part of the Section 4.2: Phase Transition in Liquid Formulations. An overview of the discussed image-based analytical techniques for each subsection is shown in Fig. 4, including a representative image for each discussed technique.

4.1.1. Subvisible particle characterization in liquid formulations

For liquid formulations, formation of subvisible particles is an undesired phenomenon and is considered a critical quality attribute (CQA) on its own [52,150,151]. There is not a single analytical technique that captures all aforementioned size ranges, and different techniques are therefore employed to cover different size ranges [152]. Regardless of the size range, analytical techniques employed for subvisible particle characterization should be able to detect, identify, and quantify particles [153]. Non-imaging-based techniques used for subvisible particle detection include, but are not limited to, dynamic light scattering (DLS), light obscuration (LO), and asymmetrical flow field flow fractionation [154–156]. Non-imaging-based techniques are able to generate information on particle size, its distribution, and concentration, but often lack the ability to provide data on particle identity and characteristics.

Table 1
Overview of literature per application and the employed electromagnetic spectrum (EMS) section.

Application	EMS section	Method	Information content	References
Sub-visible particle characterization	Visible light	FIM	Size (>0.75 μm [52–54])	[55–61]
In liquid formulations			Morphology	
		BMI	Size (>2 μm [61])	[62,63]
		IFC	Size (0.1–100 μm [64])	[64–66]
			Composition and compound distribution	
		NTA	Size (30 nm – 1 μm [67])	[67,68]
In solid formulations		Bright field	Size (>10 μm [69,70]), Morphology	[69–73]
		Digital holography	Size (20 μm – 3 mm [74]), Morphology	[74]
Phase transitions in liquid formulations	UV	UV-light imaging	Size, morphology, composition	[75–77]
	Visible light	Bright field		[78–87]
		Stereo imaging		[88]
		Fluorescent labeling		[89–96]
		Cross polarized light	Crystal presence	[97–99]
	NIR	SONICC	Crystal identification	[100–102]
	MIR	ATR-FTIR	Structural state of proteins	[103,104]
			Protein species	
Conformational stability	MIR	(ATR-)FTIR	Structural state of proteins	[105–107]
Drying effects	MIR	Thermography	Object temperature	[108–114]
Process parameters		SDD	Temperature distribution	[115,116])
	Visible light	SDD	Droplet geometry	[117–119]
Residual moisture content and homogeneity	NIR	Chemical imaging	Moisture content	[120,121]
	NIR	SDD	Compound distribution	[122–124]
		Raman	Compound distribution	[125]
Cake appearance	Visible light	Bright field	Cake height, glassiness, uniformity, color	[126,127]
Freeze/thaw effects	Visible light	Bright field	Protein long-term stability	[128–133]
			Freezing and thawing temperature	
	MIR	Thermography	Sample and ice nucleation temperature	[129,134–136]
			Ice crystal distribution	
	NIR	Raman	Compound distribution	[137,138]
Protein cloud-point temperature	Visible light	Bright field	Sample turbidity	[129,130,139]
Surface tension	Visible light	ADSA	Droplet shape	[140–144]

Abbreviations
EMS: electromagnetic spectrum, FIM: flow imaging microscopy, BMI: backgrounded membrane imaging, IFC: imaging flow cytometry, NTA: nanoparticle tracking analysis, UV: ultraviolet, NIR: near infrared, MIR: mid-infrared, ATR-FTIR: attenuated total reflection Fourier transform infrared, SONICC: second order nonlinear optical imaging of chiral crystals, SDD: single droplet drying, ADSA: axisymmetric droplet shape analysis

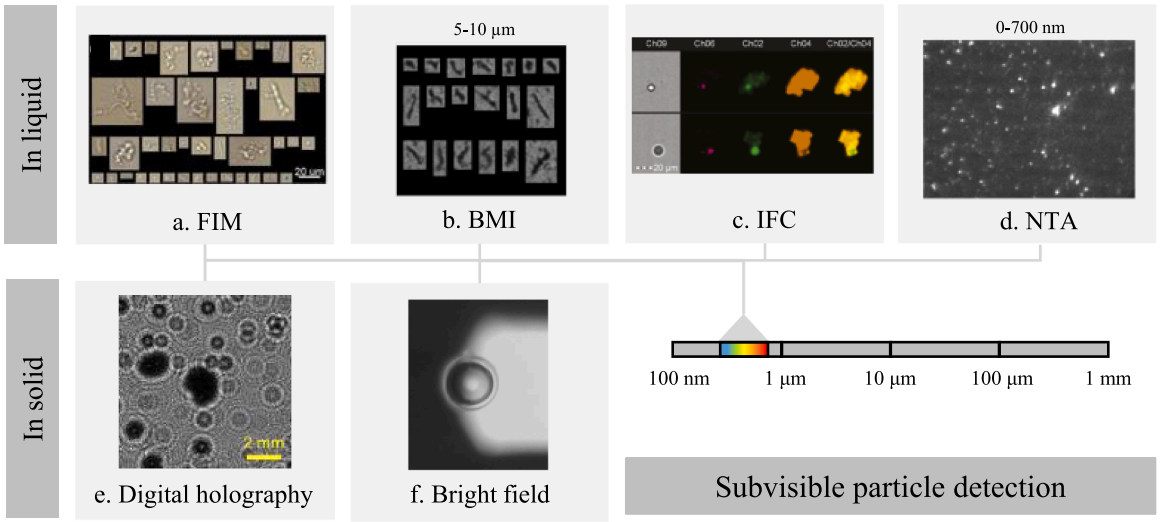

Fig. 4. Imaging examples for sub-visible particle characterization in liquids (upper row) and in solids (bottom row). The shown images are obtained with (a) flow imaging microscopy (FMI) [55], (b) backgrounded membrane imaging (BMI) [62], (c) imaging flow cytometry (IFC) [64], (d) nanoparticle tracking analysis (NTA) [67], (e) digital holography [74], and (f) bright field imaging [70] .

Most imaging-based techniques have the advantage to be able to quantify particle characteristics and identify the particles as well.

A widely applied imaging-based technique is flow imaging microscopy (FIM), which captures visible light images of a liquid sample as it flows through a cell and it allows for particle characterization down to 0.75 µm [52–54]. Most recent studies employing FIM for subvisible particle characterization focus on data processing and data evaluation automation, and some will be highlighted in this section to indicate the variety of approaches and applications. One of these studies was able to use FIM data to separate drug formulations that led to severe adverse reactions and formulations that did not, based on differences in particle morphology properties, such as diameter and circularity [56]. In other studies, classification algorithms based on FIM data were developed to accurately distinguish between protein and silicon particles [57], or silicon and non-silicon particles [58]. FIM data in combination with advanced and automated analysis is also used to identify the root cause of particle formation. For instance, recent applications of FIM data coupled to advanced classification algorithms showed the ability to elucidate the stressor origin, such as agitation or freeze/thaw stress, of particles found in pre-filled syringes [59] or monoclonal antibody formulations [60]. Yet another study presented how supervised machine learning of convolutional neural networks allows for the classification of process conditions or stress states of subvisible particle from FIM data [61]. Not only individual particle images can be classified, also particle populations have been used. In this concept, a particle population is compared to a baseline particle population to detect deviations and to establish the root cause of the found deviation [55]. Representative images of this study are shown in Fig. 4a. The diversity of angles for data evaluation and application reflects the strengths of FIM for subvisible particle characterization and how it supports further understanding of subvisible particle formation.

A more recently developed imaging-based analytical technology for subvisible particle characterization is backgrounded membrane imaging (BMI), where visible light images are taken of a membrane before and after a liquid sample is dispensed on top and filtered through the membrane. The empty membrane image is used for background subtraction, thereby elimination background information and thus enhancing particle detection. BMI was developed to overcome limitations encountered for LO and FIM, such as cleaning issues, a low sample throughput, and large sample volumes [62]. Two recent studies performed comparability experiments with BMI, LO, and FIM, which highlighted the higher sample throughput (96 samples), low sample volume requirement (only 20 µL instead of several 100 µL), and ability for particle detection despite an almost similar refractive index of the particle and its surroundings when using BMI [62,63]. An image obtained with BMI is shown in Fig. 4b. Even though BMI has shown these advantages, it was stated that BMI still requires further development to become competitive when it comes to generating morphological information and the detection of particles with homogeneous properties, such as polystyrene standard particles [62,63].

Fluorescent labeling and subsequent imaging, referred to as imaging flow cytometry (IFC), is also applied for subvisible particle detection. It was stated that IFC is a simpler method for protein identification compared to FIM (via dyes instead of particle characteristics), while it also remains high-throughput and automated [65,66]. Similar to FIM, a recent study showed that IFC is able to accurately classify and size silicon droplets and protein aggregates [64]. Moreover, this study reported on how IFC provides a visual representation of proteins agglomerating on the silicon droplet surface [64]. A representative IFC image is shown in Fig. 4c. Nevertheless, IFC is dependent on a fluorescent signal, which requires additional sample preparation and potential product interference, and this technique cannot provide data on particle characteristics.

A fundamentally different imaging approach to identify nano- and submicron particles is nanoparticle tracking analysis (NTA, detection from 0.03 µm to 1 µm) [67,68]. During NTA, cameras are used to track the Brownian motion of particles by means of laser illumination. The Brownian motion is used to determine the diffusion coefficient, which, in turn, is used to calculate to the hydrodynamic radius via the modified Stokes-Einstein equation [157]. An example of a NTA image is presented in Fig. 4d. Even though this technique was found to be suitable for protein aggregate detection [67,68,158], NTA solely provides information on the number-based size distribution as well as a semi-quantitative particle concentration, and not morphological particle characteristics. Moreover, the accuracy of NTA was shown to be dependent on the number of detected particles [67], camera settings [159], and the presence of large particles, which can adversely influence the measurement [158].

4.1.2. Subvisible particle characterization in solid formulations

Subvisible particle characterization for solid formulations is applicable for freeze- and spray-dried formulations. Dried particles for pulmonary drug delivery should lie between 1 µm and 5 µm (depending on the application) [160,161] and representative work focused on enhancing biopharmaceutical storage stability by spray-drying report a

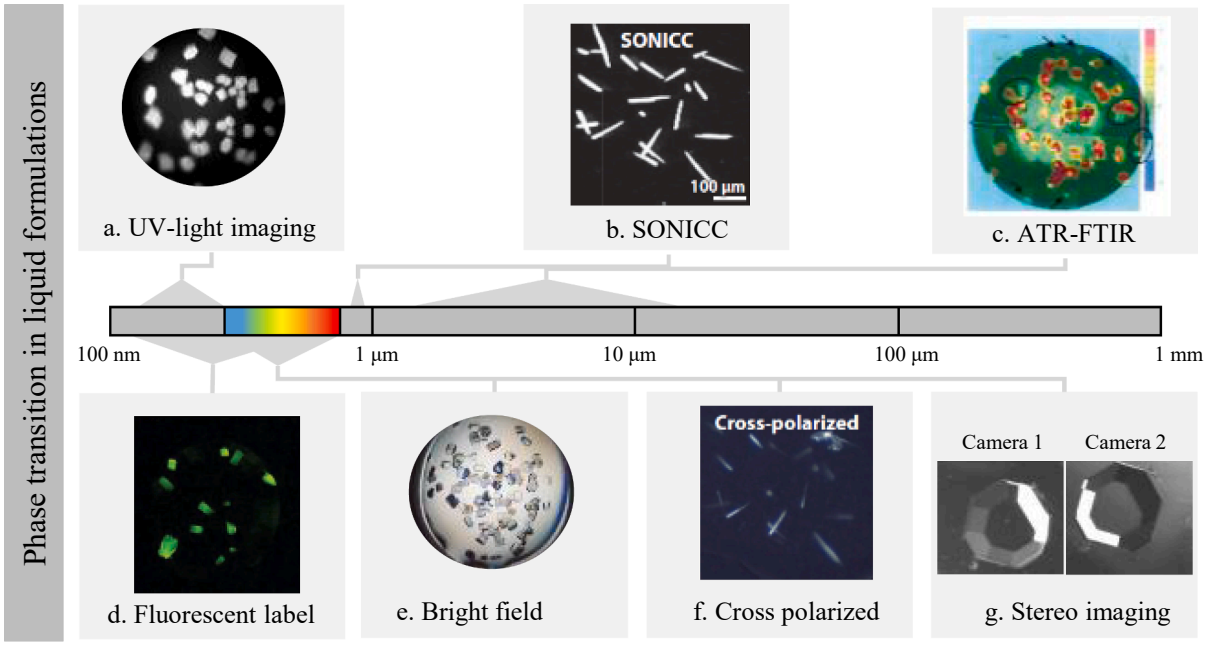

Fig. 5. Imaging examples for detection of phase transitions in liquid formulations. The shown images are obtained with (a) UV-light imaging (image obtained from own database), (b) second order nonlinear optical imaging of chiral crystals (SONICC) [101], (c) attenuated total reflection Fourier transform infrared (ATR-FTIR) chemical imaging [103], (d) fluorescent labelling imaging [89], (e) bright field imaging (image obtained from own database), (f) cross-polarized light imaging [101], and (g) stereo imaging [88].

particle size between approximately 1 µm to 30 µm [162,163]. Thus, the obtained dry powder particles are considered to fall in the category of subvisible particles.

Particle size, distribution, and morphology are of importance, as these properties determine pulmonary drug product performance [164] or reconstitution behavior of dried products [165,166]. In addition, the pore structure of freeze-dried particles is evaluated as pore size regulation can optimize the drying steps of the process [167]. These particle properties are influenced by process parameters, such as drying air temperature for spray-drying or freezing rate for freeze-drying [168], and formulation composition, such as feed concentration [169]. Reported non-imaging-based analytical techniques used for the determination of particle size and distribution can be similar to liquid formulations, such as laser diffraction [71]. However, non-imaging-based analytics suffer from similar disadvantages too, such as the inability to obtain information on particle morphology. An imaging-based technique used to assess the particle morphology after spray-drying is visible light microscopy [69–73]. A visible light image of a spray-dried particle is shown in Fig. 4f. However, the applicability of light microscopy for spray-drying studies is limited by the depth of field [74]. Digital holography imaging was applied in a field other than biopharmaceutical formulation research for droplet size (down to 20 µm) and droplet size distribution measurements have shown to improve depth of field limitations [74]. An example of such a digital holography image is shown in Fig. 4e. Though the depth of field is improved with digital holography, the application for biopharmaceutical formulation research is not established. In addition to the depth of field, a more restricting factor for visible light imaging is resolution, as the mentioned particle sizes (1–30 µm) are near or below its detection limit [156]. To overcome the resolution limitation, scanning and transmission electron microscopy (SEM/TEM) are often used to provide (morphological) particle information of spray and freeze-dried particles [170]. Although SEM and TEM are imaging techniques, the techniques are fundamentally different from the imaging techniques discussed in the review (SEM and TEM use electron beams instead of photon beams) and are therefore considered out of scope of this review.

4.2. *Phase transitions in liquid formulations*

This section on phase transitions in liquid formulations covers imaging approaches used for the evaluation of protein phase diagrams, a methodology used to assess protein phase behavior as a function of varying conditions, such as pH, additives, and product concentration [171]. This experimental approach is employed to identify crystallization conditions [172–174] and generate an understanding of protein phase behavior in liquid formulations [78,175]. Imaging is the main analytical technique to evaluate protein phase diagrams [176], where crystallization studies focus on finding protein crystals (Fig. 4D) and protein phase behavior studies focus on the identification of any type of phase transition, such as liquid–liquid phase separation or skin formation [177,178]. Similar to subvisible particle characterization, the presence of non-protein particles, such as dust, is also of interest for both crystallization and phase behavior studies. Thus, this section includes image-based techniques applicable for visible (non–)protein particle characterization in liquid formulations, but is not explicitly defined as such, as not all protein phase diagram results are composed of visible particles. A set of selected examples of images for different techniques discussed in this section are shown in Fig. 5.

Visible light is the most widely employed light source to evaluate protein phase diagrams (Fig. 5e). Adjustments in all steps of the image analysis workflow are explored to optimize and automate protein phase behavior evaluation. Automated image acquisition was achieved by implementation of robotic imaging systems and the use of liquid handling stations increased the sample throughput up to 1536 well plates [78,79,179]. Self-built multi-well plate imaging equipment was presented as an economic optimization, to facilitate a wider implementation of protein phase diagram imaging systems [80,81,83]. Information retrieved by image acquisition is expanded by increasing the acquisition frequency, where data extraction from visible light imaging was performed over the entire time course of an experiment, instead of solely endpoint images [84,86,87].

Most studies aiming to advance protein phase behavior screenings report on image acquisition hardware adjustments, where the imaging configuration is altered or different light sources are implemented. For

example, light polarization was used to specifically find crystallized proteins, as crystals are birefringent [97–99]. In Fig. 5f an image obtained with light polarization is shown. Another example is the use of a two-camera configuration to perform stereo imaging of protein crystals in the visible light range. This allows one to characterize protein crystal properties, such as face growth rate or surface area, via a three-dimensional image [88,180]. An example of a stereo-image is shown in Fig. 5g. Despite the ability to obtain three dimensional information on crystals, visible light stereo imaging is not widely applied for phase transition studies. This may be a result of the complex computational steps required to perform data evaluation or the sensitivity of the configuration [180]. The implementation of different light sources covers almost the entire range of the electromagnetic spectrum discussed in this review. UV light is used to distinguish between protein and non-protein phase states, by making use of intrinsic protein fluorescence [76,77]. A UV-image of crystallized lysozyme is shown in Fig. 5a. Low-cost configurations were demonstrated for UV-based imaging, such as the on-chip UV holographic crystal imaging platform developed by Daloglu et al. [75]. Even though the UV-range is most often used to identify proteinaceous material, intrinsic protein fluorescence in the visible light range was demonstrated as well [85]. However, among other disadvantages, the degree of UV-auto-fluorescence differs between proteins, and in some cases auto-fluorescence is even non-existing [181]. This complicates the development of a general applicable approach for protein phase behavior screenings. One of the solutions for the auto-fluorescence problem is the use of trace fluorescence labeling of the protein (extrinsic fluorescence), which allowed for a clear distinction between protein molecules bound to the fluorescent compound and the other solution components [89,90,93,96]. An image obtained with extrinsic fluorescence is shown in Fig. 5d. Miniaturization and simplification of extrinsic fluorescent imaging was also demonstrated, such as a chip-based approach [91] and configurations using mobile phones as acquisition device [92,94,95]. Even though fluorescent labeling simplifies protein identification, addition of fluorescent labels is often undesired due to additional sample preparation steps.

Light sources using longer wavelengths than visible light were successfully implemented as well. A relatively new technique is called second order nonlinear optical imaging of chiral crystals (SONICC), which uses a 800 nm light source [100–102]. An image obtained with the SONICC technique is shown in Fig. 5b. This technique showed useful for crystal identification but it did not provide any additional information for other possible phase states. Another technique in the IR range, ATR-Fourier Transform IR (ATR-FTIR) chemical imaging, was also shown as a valuable tool [103,104]. This technique uses the protein-specific amide II band absorbance in the ATR-FTIR spectrum to identify proteins, up to six samples at once (shown in Fig. 5c) [103]. The chemical information could potentially distinguish between different structural states of a single protein species or between different protein species, which could be useful to identify targeted phase transitions of complex protein mixtures. The last section of the electromagnetic spectrum that falls within this review is the THz range. The THz range has not been applied yet for the purpose of screening protein phase behavior as a function of different environmental conditions, but it is applicable to determine polymorphic crystal forms [48]. This information could be a useful feature to distinguish between different crystal types.

Next to image acquisition, a route for phase state identification improvement can also be found via the pre-processing, segmentation, and description step in the image analysis workflow. A concise summary of work reporting on different approaches for each step in the image analysis workflow can be found in the Chapter 4 of the book Data Analytics for Protein Crystallization by Pusey and Aygün [182]. What the authors of this review would like to emphasize in addition to the summary provided by Pusey and Aygün, is the general trend towards targeted human interpretation. Targeted human interpretation means that advanced computational approaches are used to minimize subjective data evaluation by operators and/or scientists, but still allow room for interpretation to gain fundamental insights. This trend becomes evident from the development of pattern recognition algorithms [183] and data-dependent descriptors [184], instead of describing an image by (enormous [185]) feature sets, obtained from global images, local sections [186], or even individual pixels [187]. This is also shown by the exploration of different light source combinations instead of using just one light source to capture all characteristics [84,188,189]. Lastly, it has become apparent that a perfect protein phase state classification algorithm is hard to come by. Thus, by understanding the added value of (multiple [93,190]) classifiers, one can make proper use of the probability of correct protein phase state classification based on imaging data, for example by directing human interpretation to low probability classifications [84].

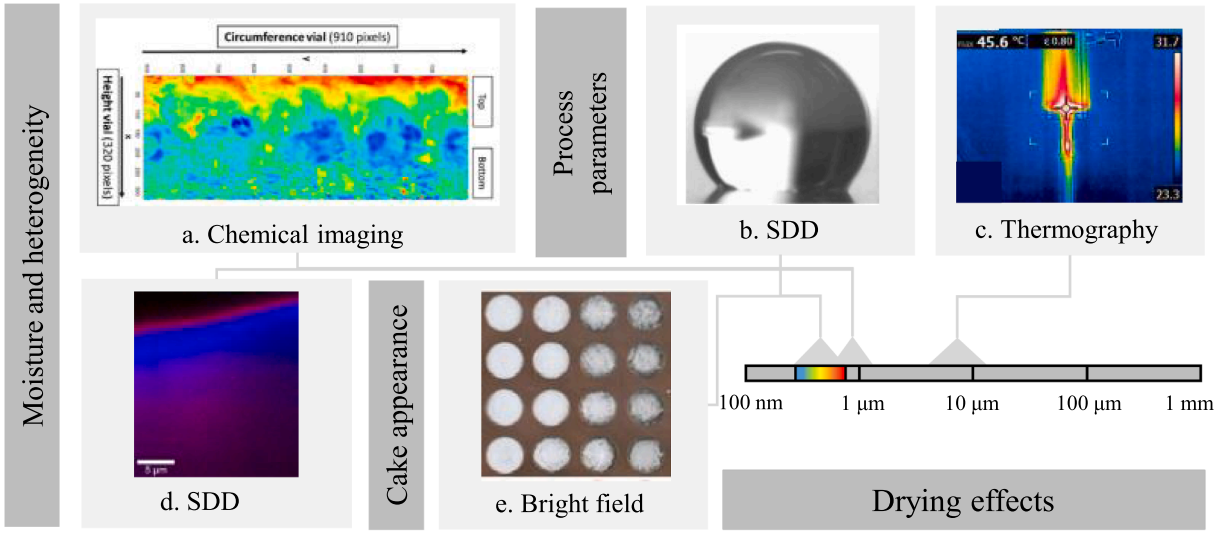

Fig. 6. Imaging examples for the evaluation of drying effects. Images are obtained with (a) chemical imaging based on Raman scattering [120], (b) single droplet drying with bright field imaging [118], (c) thermography [163], (d) single droplet drying chemical imaging based on Raman scattering [123], and (e) bright field imaging [127]. Image (a) and (d) are representative imagines to evaluate residual moisture and compound heterogeneity, (b) and (c) are representative for process parameter evaluation, and image (e) for cake appearance evaluation.

4.3. Drying effects

Protein-based biopharmaceutical products are dried to enhance shelf-life [162,191–193] or to obtain a biopharmaceutical formulation applicable for pulmonary drug delivery [160,168,194]. Dry powder biopharmaceuticals are mainly produced by means of freeze-drying (also known as lyophilization) [195,196]. This procedure includes three steps, namely (1) freezing, (2) sublimation of ice (primary drying) and (3) desorption of water (secondary drying) [192]. Freeze-drying is found to be relatively expensive due to its time-consuming and batch-based operations, and the capital investment for the cryogenic facilities. The second most often applied drying method, spray-drying, is seen as an alternative approach as it can overcome the disadvantages mentioned for freeze-drying [197]. Spray-drying produces dry powder by atomizing a liquid feed into droplets within a hot medium, such as steam, resulting in the evaporation of the solvent from the droplets [198]. However, any type of water removal processing step can induce protein destabilization [192]. Drying may impair conformational, colloidal, and chemical stability, and it may result in the removal of functional water molecules [196,199–201]. To ensure a stable, safe, and functional end product, the influence of drying process parameters on product quality needs to be evaluated during the development of dry powder biopharmaceutical formulations. In this section, the role of imaging during the drying step of freeze and spray-drying is presented. The role of imaging during the freezing step of freeze-drying will not be covered here, as this is covered in Section 8: Freeze/Thaw Effects. The following subsections present imaging-based approaches used to extract information on critical drying process parameters. In addition, three product quality attributes will be discussed, namely residual moisture, compound homogeneity, and freeze-dried cake appearance. A selection of images obtained with techniques discussed in this section are shown in Fig. 6.

4.3.1. Drying process parameters

One of the critical processing parameters for freeze- and spray-drying is temperature. Commonly employed non-imaging-based temperature measurement techniques for freeze-drying are thermocouples and resistance temperature detectors, which are invasive and require a subjective selection of a few samples to be measured [202]. Thermal imaging is non-invasive and it offers spatial temperature readings, a characteristic applicable for analyzing multiple samples at once. In addition, thermal imaging can simultaneously determine the temperature variations within a sample. The first implementation of a thermal camera on the outside of a freeze-drying chamber was described by Emteborg et al., which resulted in the quantification of temperature variations between formulation vials during the primary drying step [108]. Thermography also facilitated the estimation of kinetic freeze-drying parameters, where a study by Lietta et al. reported on the estimation of the end of primary drying (sublimation), the heat transfer coefficient, and the resistance of the dried product to vapor flux [109]. Not only drying process parameters were extracted by means of imaging, Colucci et al. showed how to use thermal and visible light imaging to determine temperature deviations in the entire drying process [113,114]. Work was also reported on developments for the computational side of image analysis, where a real-time data extraction workflow for enhanced vial detection and image segmentation based on thermographic data was presented [112].

The implementation of a thermal camera enhanced process understanding, but it also led to discussion on camera placement. A freeze-drying chamber often consists of multiple shelves and multiple vials per shelve. Measuring from the top of the chamber results in the loss of information from the shelves below the top shelf, while measurements from the side do not capture vials at the back of the chamber. Thus, thermography is able to perform noninvasive temperature measurement for more samples than non-imaging-based techniques, it is not able to account for all nonuniformity due to the technical limitations of the drying equipment. To overcome nonuniformity of batch-freeze-drying (among other limitations), continuous spin freeze-drying was developed [203]. This freeze-drying method facilitates vial-per-vial evaluation and was used in combination with thermography in a study performed by Van Bockstal et al.. This work resulted in the identification of the primary drying end point and mass transfer parameters useful during product and process development [110].

For spray drying, a recent study showed how thermal imaging was implemented to monitor the spraying nozzle temperature. The respective work visualized temporal and spatial nozzle temperatures (Fig. 6c), which led to identification of the root cause of lysozyme's reduced activity after spray-drying [163]. Such a study requires a benchtop or industrial scale spray dryer, which is not ideal for (early stage) characterization studies due to the required amount of protein material. To minimize material consumption, spray-drying process parameters are often evaluated via single droplet drying (SDD) experiments. In SDD experiments a single sessile, free flight, or levitating droplet is produced and dried over time to mimic spray-drying conditions [118,204]. A representative image of a sessile drop is shown in Fig. 6b. The selection of a particular SDD method affects the observed kinetics, where each SDD method has its own advantages and disadvantages [205]. Even though SDD is applicable to retrieve an understanding of spray-drying on a benchtop or industrial scale, particle size and particle processing time obtained via SDD experiments is not identical to large scale spray-dryers. Thus, information obtained on kinetics and morphology should solely be seen as an additional source of fundamental insights [205,206]. Despite the deviations between SDD and larger scale spray drying, process parameters for spray-drying have been modeled based on a SDD data. Single droplet thermographic measurement have been performed [115,116], but also visible light imaging was applied for drying process understanding and modeling [117,118]. Visible light imaging was used to extract the geometry of drying droplets over time and employed to model the drying process, where the resulting models were able to predict post-spray-drying enzyme activity [118,119]. It would be interesting for the field of biopharmaceutical formulation research to determine the applicability of such SDD-based models for protein stability prediction.

4.3.2. Residual moisture content and homogeneity

It has been shown in multiple studies that the required amount of residual moisture to ensure product stability is protein-specific and, thus, the lowest amount of residual moisture is not always desired [207,208]. Moreover, the distribution of residual moisture is also of interest, as an uneven distribution of the residual moisture is a sign of local overdrying, thereby creating a possible destabilizing environment in overdried regions [209]. Thus, to determine the quality of the dry powder and the product itself, it is important to measure the residual moisture content, moisture homogeneity as well as the protein state and homogeneity.

Examples of non-imaging-based techniques to determine the residual moisture after drying are Karl Fischer titration [210] or thermogravimetry (recording mass as a function of temperature) [211], both destructive and invasive methods. This led to the implementation of IR spectroscopy as a noninvasive alternative [212,213], where water interference in the IR region is considered an asset instead of a nuisance, as is the case when studying protein structural elements with IR spectroscopy. Imaging-based techniques were derived from the spectroscopic approaches to introduce the spatial information in addition to the spectral data. The study by Brouckeart et al. mentioned in Section 7.1, which employed spin freeze-drying and thermography, additionally implemented chemical imaging in the NIR region to determine the moisture content and compound homogeneity for mannitol-sucrose formulations [120]. A representative image is shown in Fig. 6a. NIR imaging was also used to determine sugar crystallization in addition to residual moisture for mannitol/sucrose/lysozyme or bovine serum albumin mixtures after freeze-drying and after storage of the freeze-dried

formulations [121]. A study focused solely on product distribution by chemical imaging based on Raman scattering showed the influence of glycerol on lysozyme/trehalose formulations during freeze-drying [125]. For spray dried formulations, SDD experiments used Raman imaging to determine the residual moisture and homogeneity of dextran/sucrose mixtures within the spray dried particle [122]. SDD chemical imaging has also been employed to study the distribution of different protein/sugar formulations, such as lysozyme/mannitol [124] and bovine serum albumin/lactose (Fig. 6d) [123]. Information obtained with chemical imaging on residual moisture content as well as moisture and product distribution generates a broader understanding of the influence of formulation parameters on particle engineering. This knowledge can be applied to enhance product stability and product functionality via formulation optimization on a particle level.

4.3.3. Cake appearance

After freeze-drying, the resulting dry powder product is referred to as the cake. The appearance of the cake is important as it reflects the quality of the freeze-drying process and it is considered a critical quality attribute by the health authorities [214]. Undesired cake properties are, for instance, cake collapse (leading to a longer reconstitution time) and meltback (indicating an incomplete sublimation step) [215]. Visible light imaging evolved from the traditional visual inspection as an imaging-based analytical approach for cake appearance evaluation. Similar to crystallization and phase transition studies, cake appearance evaluation has long been a subjective approach, performed by operators and/or scientists. This initiated the development of machine learning approaches that are able to evaluate the cake appearance, and thus its quality. A high-throughput image analysis algorithm based on visible light images was developed by Trnka et al. to automatically evaluate cake collapse, glassiness, uniformity, and color [126,127]. A representative image is shown in Fig. 6e. The workflow developed by Trnka et al. is applicable for formulation design screening purposes only, as freeze-drying and subsequent image analysis was performed in multi-well plates and not in formulation vials.

Visible light imaging is fast and relatively simple to implement, but its main limitation is that visible light imaging only evaluates the exterior of the cake. Haeuser et al. published work comparing a variety of imaging-based techniques to evaluate the applicability for capturing the interior of the cake [216]. For this, Haeuser et al. used visible light imaging and microscopy, three-dimensional laser scanning, scanning electron microscopy, and microcomputed tomography (μCT) to evaluate freeze-dried formulations with a cake volume between 5.25 cm^3 and 8.43 cm^3 and a diameter of approximately 28 mm. Out of these techniques, μCT was highlighted as a imaging technique with potential for the application of cake appearance, as it is able to perform non-invasive qualitative and quantitative measurements through glass [216,217]. However, this technique falls outside of the electromagnetic spectrum range discussed in this review and will therefore not be further discussed.

4.4. Freeze/thaw effects

Freezing and thawing are a part of biopharmaceutical production processes, where it is used for intermediate holding during processing, transport, and long-term storage of liquid formulations. However, freeze/thaw (F/T) cycles can affect proteins' conformational stability resulting in cold denaturation [218] or denaturation at the ice interface [219], thereby compromising protein function, efficacy, and product safety. Moreover, freeze concentration during F/T cycles may also change the environmental conditions in such a way that it induces conformational, colloidal, or chemical instability [220]. Formulation composition and F/T processing parameters, such as cooling rate or minimum temperature, are optimized to minimize these effects. On the right side of Fig. 7 representative images are shown which were used to study freeze/thaw effects.

Studies performed by Wöll et al. employed visible light imaging for high-throughput and low volume screening of long-term stability effects induced by F/T cycles as a function of process parameters, such as cooling rate and F/T cycle number, and formulation parameters, such as buffer pH and salt concentration [131–133]. Visible light imaging is also able to detect temperature-induced phase transitions during a F/T cycle.

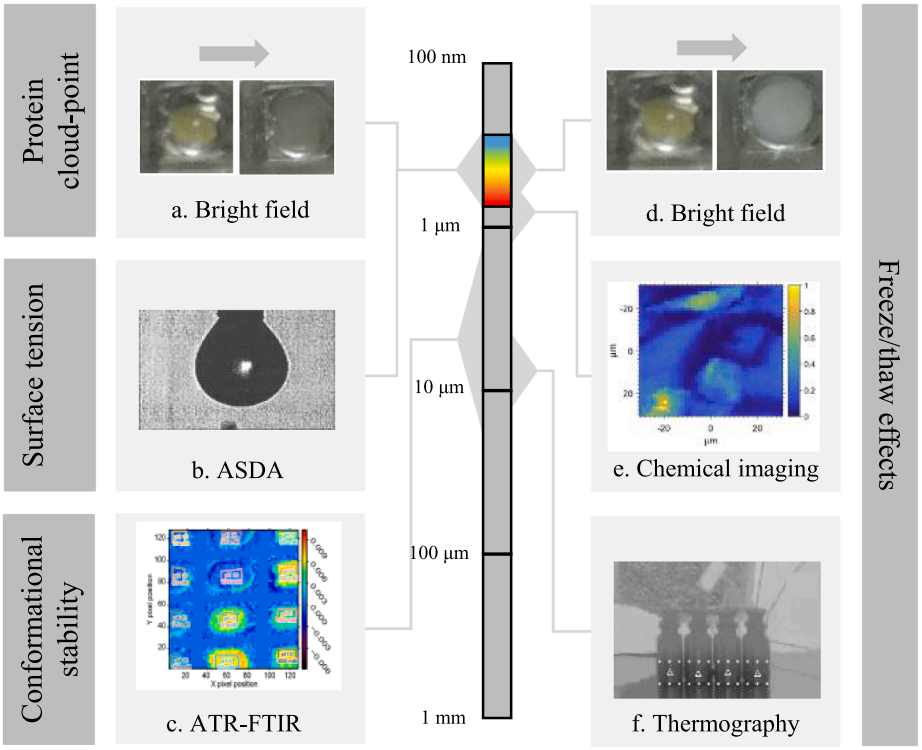

Fig. 7. Imaging examples for the evaluation of the (a) protein cloud-point temperature, (c) surface tension, (e) conformational stability, and (b, d, f) freeze/thaw effects. Images are obtained with (a, b) bright field imaging (images obtained from own databse), (c) axisymmetric droplet shape analysis (ASDA) with bright field imaging [143], (d) chemical imaging based on Raman scattering [138], (e) attenuated total reflection Fourier transform infrared (ATR-FTIR) chemical imaging [105], and (f) thermography [135].

The pixel intensity difference between the starting image and subsequent images captures during a F/T cycle showed distinct points in the intensity difference-temperature profile, of which two were traced back to freezing and thawing points of lysozyme formulations (Fig. 7b) [130]. A comparable imaging approach extracted the mean pixel intensity of visible light images to determine the freezing and thawing temperature during cryopreservation of cells, which may be of interest for cell-based biopharmaceutical products [128]. Determination of these transition points does not yield direct information on product quality, but correlation studies that link thermal transition points to stability or functionality allows one to adjust F/T process parameters and formulation composition accordingly.

In addition to freezing and thawing temperature, there are other characteristics of interest during freezing of protein-based biopharmaceuticals that are extractable via imaging, such as the ice nucleation temperature and ice crystal distribution. Ice nucleation is the spontaneous formation of ice crystals in super-cooled solutions, which affects the ice crystal distribution and subsequently the drying time and product quality during freeze-drying processes [165]. Thermography is able to detect ice nucleation as it is an exothermic reaction, which results in a sudden increase of temperature up to the equilibrium freezing temperature of the sample, where the difference may lie in the order of magnitude of ten degrees Celsius [167]. The ice crystal distribution can be determined directly with imaging, via techniques such as scanning electron microscopy [170] and micro-computed X-ray tomography [217]. However, these methods fall outside the scope of this review. Imaging techniques that fall within the range of this review facilitate only an indirect approach to estimate the ice crystal distribution. The estimation of the ice crystal distribution is generated via empirical and/or mathematical models based on process parameters [221]. Colluci et al. employed thermography to capture temperature profiles within the frozen product and freezing front rates (Fig. 7f). This information was used to estimate the ice crystal size distribution at the end of the freezing step of the freeze-drying process [134,135]. Thermography has also been used to adjust computational fluid dynamic simulations [136]. These simulations are employed to predict the temperature and solute concentration development in sample containers during freezing. The solute distribution within frozen samples during freeze-drying has also been studied with Raman imaging. Raman images were visualized ratios between three components, namely ice, lysozyme, and sugar (sucrose and trehalose), which was used to elucidate the stabilizing effects of these sugars during freeze-drying [137,138]. A representative Raman scattering-based image is shown in Fig. 7d.

4.5. Conformational stability

Conformational stability refers to the structural stability of the folded protein molecule, which is often monitored during characterization studies. This is done as structural instability can lead to loss of product functionality or it can induce adverse immune reactions. One of the biophysical properties that represents conformational stability is the melting temperature (T_M), where structural unfolding of a protein molecule is monitored over a temperature gradient as a function of different environmental factors, such as pH or osmolality [222]. The differences in temperature at which unfolding occurs allows one to interpret the relative degree of conformational stability. Conformation stability can also be monitored without a temperature gradient. In such experiments, proteins' secondary structure motifs are identified and compared between different formulation parameters. Examples of commonly applied non-imaging-based techniques to monitor conformational stability are DLS [223,224], dynamic scanning fluorescence (DSF) [225], circular dichroism (CD) [226], and Raman [227] or IR spectroscopy [228]. Imaging-based assessment of conformational stability is done with chemical imaging, allowing one to perform dynamic measurements and to distinguish and quantify different proteins and mono/multimeric protein species, which cannot be done with light scattering and fluorescence techniques. Raman and IR spectroscopy also possess these properties, but chemical imaging has the ability to capture multiple samples in one image and to visualize the species-distribution within the sample as a result of the spatial dimension.

The first application of chemical imaging to investigate conformational stability of monoclonal antibodies was shown by Boulet-Audet et al., where monoclonal antibodies were investigated as a function of a multitude of environmental factors in a high-throughput manner (twelve samples per measurement) [105]. A representative image is shown in Fig. 7e. A similar imaging throughput was reached by De Meutter et al., where protein microarrays were used to analyze the secondary structure by means of chemical imaging for a multitude of proteins [106]. Another study employed ATR-FTIR imaging to determine structural differences between monoclonal antibody species in the bulk solution and precipitated monoclonal antibodies (six samples per measurement) [107]. Up until this moment, there are only a few chemical imaging studies performed to assess conformational stability for biopharmaceutical formulations, but examples for small molecules [229] and polymers [230] exist. Nevertheless, the reported work on biopharmaceutical-relevant proteins illustrates the detailed and valuable spatial information that chemical imaging can bring to the field. Moreover, chemical imaging provides a technology to perform high-throughput IR-spectroscopy by imaging multiple samples at once.

It should be noted that the aforementioned studies were performed with the MIR region of the electromagnetic spectrum, as it known to represent secondary structure motifs (see Section 2.4). Though not yet realized, chemical imaging in the THz range may be of interest for conformational stability assessment, as thermodynamic changes relevant during protein unfolding are detectable in the THz range [231]. For example, the effect of different structural conformations of bovine serum albumin on the surrounding water molecules was detected with THz time-domain spectroscopy [232]. The inverse analysis, where the THz range is employed to determine the protein's conformational changes, was shown for bovine serum albumin [233] and pepsin [234]. These recent spectroscopic studies show promising results for potential THz imaging applications with regard to protein conformational stability.

4.6. Protein cloud-point temperature

Temperature recordings can also be a part of an analytical method, as is done for the determination of the protein cloud-point temperature (T_{Cloud}). The T_{Cloud} is defined as the temperature at which a solution displays liquid–liquid phase separation, where the protein-dense phase causes a change in solution turbidity (see Fig. 4H). The temperature value at which this phenomenon occurs depends mainly on the protein–protein interaction strength [235], and can be used to assess colloidal stability [236]. Imaging-based approaches have been developed to determine the change in solution turbidity as a function of temperature [130,139], which serve as an alternative for visual inspection [237], light transmittance [238], spectroscopy [239,240], and light scattering [241–244]. Several approaches have been tested to detect the turbidity change, such as identifying a decrease in mean gray pixel intensity [139], an increase in binary intensity difference compared to the starting point image [130], and the total number of white pixels [129]. A representative example of turbidity change is shown in Fig. 7a. Though the information content between set ups for light transmittance, light scattering, spectroscopic, and imaging does not differ, the main benefit of employing an imaging-based approach is the hardware simplicity, measurement speed, and its compatibility for miniaturization and high-throughput screening [130,139]. Between 2005 and 2020, image-based methodologies for T_{Cloud} determination have mainly evolved regarding a higher sample throughput and streamlined data analytical workflow, where more recent studies start to focus on automated data evaluation and enhanced data mining.

4.7. Surface tension

Quantification of apparent protein surface hydrophobicity is of interest during biopharmaceutical characterization studies as it provides information on the presence and strength of protein–protein interactions, protein-additive interactions, and interface/surface adsorption [245], all of which may affect product safety and efficacy. A parameter to quantify the apparent protein surface hydrophobicity is the surface tension [246,247]. There is a wide variety of analytical methods available to determine the surface tension, also referred to as tensiometry [248,249]. The axisymmetric droplet shape analysis (ADSA) method employs imaging, which can be performed with pendant droplets (hanging from a tip) and sessile droplets (deposited on a surface) [140,142]. ADSA uses the visible light range and the light source is placed behind or above the droplet, where a diffuser is sometimes placed between the light source and the sample. The droplet shape is extracted from the images, which is compared to a theoretical drop profile. The difference between the two droplet profiles allows one to quantify the surface tension, where a large deviation relates to a low surface tension, which in turn translates to a more hydrophobic protein surface. Advantages of the ADSA method compared to other surface tension measurements includes a robust analysis, the ability to perform the experiment completely automated, the possibility to run dynamic measurements, and the relatively simple implementation in the lab [250]. Surface tension measurements by means of ADSA have shown to be applicable to assess aggregation tendency as well as packaging or delivery material compatibility. Relevant example of studies using the ADSA method within the scope of this review include an investigation on the interaction of proteins with liquid–liquid as well as solid–liquid interfaces (Fig. 7c) [143], the evaluation of different insulins and their adsorption behavior as a function of concentration and pH [141], and a study on the interaction between protein A and an IgG antibody [144].

5. Future perspective

This review presents the current applicability of imaging for the development and characterization of protein-based biopharmaceutical formulations, where spatial information obtained from the UV, visible, and IR region of the electromagnetic spectrum provides a wide range of valuable knowledge. As imaging possibilities will continue to develop along the electromagnetic spectrum, it is foreseen that imaging will play a pivotal role in the establishment of novel non-invasive, high-throughput, and multiplexed analytics. The summary provided in Table 1 shows that visible light imaging was found to be suitable for most current applications, which is considered to be a result of the relatively simple configuration as well as low costs for the image acquisition devices. Contrarily, the FIR region was not applied in studies considered relevant for the field of protein-based biopharmaceutical formulation characterization and development. Nevertheless, FIR-based spectroscopic studies have been reported on, and considering the evolution of NIR and MIR imaging, it may be a only a matter of time before FIR imaging will used to capture protein hydration effects or high-order structures in a spatial dimension.

In addition to expansion of the applied electromagnetic spectrum range, it is considered key for future research to focus on covering multiple sections of the electromagnetic spectrum in a single measurement. For example, a biopharmaceutical characterization study to determine freeze/thaw effects would benefit from combining object identification by means of visible light to identify phase transitions, sample temperature distribution monitoring by thermal imaging, and molecular species identification and distribution by means of chemical imaging in a single measurement. This is regarded beneficial as it allows for mutually exclusive as well as complementary data, which will enrich fundamental understanding and simplify computer-aided analytical interpretation. Initially, such an analytical device would be technically and economically challenging, but efforts to work towards multiplexed analytical imaging possess a great opportunity to gain enhanced fundamental understanding without sample interference in a high-throughput manner. In addition to fundamental understanding, multiplexed imaging would increase the added value of imaging as PAT tool, considering that imaging in its current form is already indicated as an interesting non-invasive analytical technique for future PAT approaches [251,252].

Work covered in this review showed how recent studies focus on developing experimental instrumentation with low material usage and a high sample throughput. Consequently, the aim of imaging-based biopharmaceutical characterization studies shifts from experimental adjustments towards the computational side, where the implementation of advanced data analytics is explored to effectively use the ever-increasing data complexity. This is most evident in the studies that apply imaging to investigate phase transitions in liquid formulations, were data sets can range from hundreds up to tens of thousands of images that have to be interpreted. However, the performance of data analytical workflows and the applied (un)supervised machine learning models needs to be carefully evaluated and validated to ensure that these computational efforts actually improve the methodologies. It should be noted that the observed inconsistency between employed evaluation parameters impairs study comparability and reproducibility, as performance results are solely presented by a (subjective) selection of evaluation parameters, without proper access to the underlying data. To ensure study comparability and reproducibility of novel data analytical approaches applied to data obtained from imaging-based experimental equipment, guidelines for performance evaluation and data transparency should be formulated and maintained.

Advancement and exploration of computational workflows will remain to play an important role for analytical imaging in biopharmaceutical characterization studies. For instance, the effects of different image segmentation or transformation techniques is largely uncharted territory, and further exploration will be able to enhance the information content of already existing data. Not only segmentation and transformation will open up the available information content of the data, but also the application of deep learning approaches will be utilized more often, as it offers the ability to analyze complex data sets. Nevertheless, deep learning approaches require a data set size or data set balance that is often not obtained with biopharmaceutical characterization studies. In order to overcome such data set size challenges, implementation of data augmentation strategies (also referred to as transfer learning) is a route to consider, as these strategies provide the sample numbers and variation required to train the respective algorithms.

In conclusion, the current position that imaging obtained in the analytical toolbox employed for the characterization and development of protein-based biopharmaceutical formulations is a result of the combined effort of many research groups. Imaging has become widely accessible and applicable because these research groups developed imaging instrumentation outside the visible light range, while effectively employing the high-throughput and non-invasive nature of imaging. As seen for other analytical techniques applied for characterization and development studies in the field of biopharmaceuticals, such as spectroscopic techniques, it is not unlikely that imaging approaches will be fitted to meet the measurement requirements for monitoring during bioprocessing as PAT technology, where it may find a place in the field of non-invasive process control procedures and real-time release strategies.

Declaration of Competing Interest

The authors declare that they have no known competing financial interests or personal relationships that could have appeared to influence the work reported in this paper.

References

[1] S. Zheng, D. Qiu, M. Adams, J. Li, R.V. Mantri, R. Gandhi, Investigating the degradation behaviors of a therapeutic monoclonal antibody associated with pH and buffer species, Aaps Pharm. 18 (2017) 42–48.
[2] L. Liu, W. Qi, D.K. Schwartz, T.W. Randolph, J.F. Carpenter, The effects of excipients on protein aggregation during agitation: an interfacial shear rheology study, J. Pharm. Sci. 102 (2013) 2460–2470.
[3] S.P. Choudhari, K.P. Pendleton, J.D. Ramsey, T.G. Blanchard, W.D. Picking, A systematic approach toward stabilization of CagL, a protein antigen from Helicobacter pylori that is a candidate subunit vaccine, J. Pharm. Sci. 102 (2013) 2508–2519.
[4] B.S. Bhatnagar, R.H. Bogner, M.J. Pikal, Protein stability during freezing: separation of stresses and mechanisms of protein stabilization, Pharm. Dev. Technol. 12 (2007) 505–523.
[5] P. Holm, M. Allesø, M.C. Bryder, R. Holm, Q8 (R2) Pharmaceutical Development, ICH quality guidelines: an implementation guide (2017) 535–577.
[6] W. Wang, S. Ohtake, Science and art of protein formulation development, Int. J. Pharm. 568 (2019), 118505.
[7] Food Drug Administration, Guidance for industry, PAT-A Framework for Innovative Pharmaceutical Development, Manufacturing and Quality Assurance, in: http://www.fda.gov/cder/guidance/published. html, 2004.
[8] H. Svilenov, G. Winter, The ReFOLD assay for protein formulation studies and prediction of protein aggregation during long-term storage, Eur. J. Pharm. Biopharm. 137 (2019) 131–139.
[9] R. Wanner, D. Breitsprecher, S. Duhr, P. Baaske, G. Winter, Thermo-optical protein characterization for straightforward preformulation development, J. Pharm. Sci. 106 (2017) 2955–2958.
[10] V. Joshi, T. Shivach, N. Yadav, A.S. Rathore, Circular dichroism spectroscopy as a tool for monitoring aggregation in monoclonal antibody therapeutics, Anal. Chem. 86 (2014) 11606–11613.
[11] F. Sousa, B. Sarmento, M.T. Neves-Petersen, Biophysical study of bevacizumab structure and bioactivity under thermal and pH-stresses, Eur. J. Pharm. Sci. 105 (2017) 127–136.
[12] L. Galm, S. Amrhein, J. Hubbuch, Predictive approach for protein aggregation: Correlation of protein surface characteristics and conformational flexibility to protein aggregation propensity, Biotechnol. Bioeng. 114 (2017) 1170–1183.
[13] B.A. Kerwin, Polysorbates 20 and 80 used in the formulation of protein biotherapeutics: structure and degradation pathways, J. Pharm. Sci. 97 (2008) 2924–2935.
[14] P. Hanrahan, W. Krueger, Reflection from layered surfaces due to subsurface scattering, in, in: Proceedings of the 20th annual conference on Computer graphics and interactive techniques, 1993, pp. 165–174.
[15] J.R. Lakowicz, Principles of fluorescence spectroscopy, Springer science & business media, 2013.
[16] L.A. Nafie, Theory of Raman scattering, Pract. Spectros. Series 28 (2001) 1–10.
[17] M.R. Eftink, Fluorescence techniques for studying protein structure, Meth. Biochem. Anal. (1991) 127–205.
[18] R.J. Clarke, A. Oprysa, Fluorescence and light scattering, J. Chem. Educ. 81 (2004) 705.
[19] R.L. McCreery, Raman spectroscopy for chemical analysis, John Wiley & Sons, 2005.
[20] D.J. Lockwood, Rayleigh and Mie scattering, in: Encyclopedia of Color Science and Technology, Springer, New York, NY, 2016, pp. 1–12.
[21] I.R. Lewis, H. Edwards, Handbook of Raman spectroscopy: from the research laboratory to the process line, CRC Press, 2001.
[22] B. Schrader, Infrared and Raman spectroscopy: Methods and applications, VHC, Weinheim, Germany, 1995.
[23] A. Manickavasagan, H. Jayasuriya, Imaging with electromagnetic spectrum: applications in food and agriculture, Springer, 2014.
[24] F. Teale, G. Weber, Ultraviolet fluorescence of the aromatic amino acids, Biochem. J. 65 (1957) 476–482.
[25] R.F. Chen, Fluorescence quantum yields of tryptophan and tyrosine, Anal. Lett. 1 (1967) 35–42.
[26] J. Østergaard, UV/VIS spectrophotometry and UV imaging, in: Analytical Techniques in the Pharmaceutical Sciences, Springer, 2016, pp. 3-27.
[27] B.R. Masters, Principles of fluorescence spectroscopy, J. Biomed. Opt. 13 (2008), 029901.
[28] A. Hawe, M. Sutter, W. Jiskoot, Extrinsic fluorescent dyes as tools for protein characterization, Pharm. Res. 25 (2008) 1487–1499.
[29] T. Brosnan, D.-W. Sun, Improving quality inspection of food products by computer vision—a review, J. Food Eng. 61 (2004) 3–16.
[30] R. Jain, R. Kasturi, B.G. Schunck, Machine vision, McGraw-hill New York, 1995.
[31] D.B. Murphy, Fundamentals of light microscopy and electronic imaging, John Wiley & Sons, 2002.
[32] D. Singh, Fundamentals of optics, PHI Learning Pvt. Ltd., 2015.
[33] N. Hartshorne, A. Stuart, Practical Optical Crystallography, Chap. 4,"The Microscopic Examination of Crystals, Orthoscopic Observations," E. Arnold, Ltd., London, (1969) 154-198.
[34] J.L. Sanz, F. Merkle, K.Y. Wong, Automated digital visual inspection with dark-field microscopy, JOSA A 2 (1985) 1857–1862.
[35] E.M. Sparrow, Radiation heat transfer, Routledge, 2018.
[36] W. Wang, S. Nema, D. Teagarden, Protein aggregation—pathways and influencing factors, Int. J. Pharm. 390 (2010) 89–99.
[37] M. Vollmer, K.-P. Möllmann, Fundamentals of infrared thermal imaging, Infrared thermal imaging: fundamentals, research and applications, Wiley-VCH, Mörlenbach, 2010, pp. 1–72.
[38] M. Vollmer, K. Möllmann, Basic properties of IR imaging systems, Infrared Thermal Imaging: Fundamentals, Research and Applications, 2nd ed.; Vollmer, M., Möllmann, K.-P., Eds, (2010).
[39] H. Fabian, W. Mäntele, Infrared spectroscopy of proteins, Handbook of vibrational spectroscopy, (2006).
[40] M. Jackson, H.H. Mantsch, The use and misuse of FTIR spectroscopy in the determination of protein structure, Crit. Rev. Biochem. Mol. Biol. 30 (1995) 95–120.
[41] Y. Ozaki, Two-Dimensional Near-Infrared Correlation Spectroscopy, Near-Infrared Spectroscopy: Principles, Instruments, Applications, (2001) 163-178.
[42] C.P. Schultz, H. Fabian, H.H. Mantsch, Two-dimensional mid-IR and near-IR correlation spectra of ribonuclease A: Using overtones and combination modes to monitor changes in secondary structure, Biospectroscopy 4 (1998) S19–S29.
[43] K.B. Beć, J. Grabska, C.W. Huck, Biomolecular and bioanalytical applications of infrared spectroscopy–A review, Anal. Chim. Acta (2020).
[44] G. Reich, Mid and near infrared spectroscopy, in: Analytical Techniques in the Pharmaceutical Sciences, Springer, 2016, pp. 61-138.
[45] P.R. Griffiths, J.A. De Haseth, Fourier transform infrared spectrometry, John Wiley & Sons, 2007.
[46] S. Krimm, J. Bandekar, Vibrational spectroscopy and conformation of peptides, polypeptides, and proteins, in: Advances in protein chemistry, Elsevier, 1986, pp. 181-364.
[47] K. Buckley, A.G. Ryder, Applications of Raman spectroscopy in biopharmaceutical manufacturing: a short review, Appl. Spectrosc. 71 (2017) 1085–1116.
[48] J.A. Zeitler, P.F. Taday, D.A. Newnham, M. Pepper, K.C. Gordon, T. Rades, Terahertz pulsed spectroscopy and imaging in the pharmaceutical setting-a review, J. Pharm. Pharmacol. 59 (2007) 209–223.
[49] R.J. Falconer, A.G. Markelz, Terahertz spectroscopic analysis of peptides and proteins, Journal of Infrared, Millimeter, and Terahertz Waves 33 (2012) 973–988.
[50] S. Gunasekaran, Computer vision technology for food quality assurance, Trends Food Sci. Technol. 7 (1996) 245–256.
[51] J.M. Prats-Montalbán, A. De Juan, A. Ferrer, Multivariate image analysis: a review with applications, Chemomet. Intelligent Lab. Syst. 107 (2011) 1–23.
[52] J.F. Carpenter, T.W. Randolph, W. Jiskoot, D.J. Crommelin, C.R. Middaugh, G. Winter, Y.-X. Fan, S. Kirshner, D. Verthelyi, S. Kozlowski, Overlooking subvisible particles in therapeutic protein products: gaps that may compromise product quality, J. Pharm. Sci. 98 (2009) 1201–1205.
[53] D.K. Sharma, D. King, P. Oma, C. Merchant, Micro-flow imaging: flow microscopy applied to sub-visible particulate analysis in protein formulations, AAPS J. 12 (2010) 455–464.
[54] S. Zölls, D. Weinbuch, M. Wiggenhorn, G. Winter, W. Friess, W. Jiskoot, A. Hawe, Flow imaging microscopy for protein particle analysis—A comparative evaluation of four different analytical instruments, AAPS J. 15 (2013) 1200–1211.
[55] A.L. Daniels, C.P. Calderon, T.W. Randolph, Machine learning and statistical analyses for extracting and characterizing "fingerprints" of antibody aggregation at container interfaces from flow microscopy images, Biotechnol. Bioeng. 117 (2020) 3322–3335.
[56] A.L. Daniels, T.W. Randolph, Flow microscopy imaging is sensitive to characteristics of subvisible particles in peginesatide formulations associated with severe adverse reactions, J. Pharm. Sci. 107 (2018) 1313–1321.
[57] R. Strehl, V. Rombach-Riegraf, M. Diez, K. Egodage, M. Bluemel, M. Jeschke, A. V. Koulov, Discrimination between silicone oil droplets and protein aggregates in biopharmaceuticals: a novel multiparametric image filter for sub-visible particles in microflow imaging analysis, Pharm. Res. 29 (2012) 594–602.
[58] M. Saggu, A.R. Patel, T. Koulis, A random forest approach for counting silicone oil droplets and protein particles in antibody formulations using flow microscopy, Pharm. Res. 34 (2017) 479–491.
[59] A. Gambe-Gilbuena, Y. Shibano, E. Krayukhina, T. Torisu, S. Uchiyama, Automatic Identification of the Stress Sources of Protein Aggregates Using Flow Imaging Microscopy Images, J. Pharm. Sci. 109 (2020) 614–623.
[60] N.R. Maddux, A.L. Daniels, T.W. Randolph, Microflow imaging analyses reflect mechanisms of aggregate formation: comparing protein particle data sets using the Kullback-Leibler divergence, J. Pharm. Sci. 106 (2017) 1239–1248.
[61] C.P. Calderon, A.L. Daniels, T.W. Randolph, Deep convolutional neural network analysis of flow imaging microscopy data to classify subvisible particles in protein formulations, J. Pharm. Sci. 107 (2018) 999–1008.
[62] C. Helbig, G. Ammann, T. Menzen, W. Friess, K. Wuchner, A. Hawe, Backgrounded membrane imaging (BMI) for high-throughput characterization of subvisible particles during biopharmaceutical drug product development, J. Pharm. Sci. 109 (2020) 264–276.
[63] S.K. Vargas, A. Eskafi, E. Carter, N. Ciaccio, A comparison of background membrane imaging versus flow technologies for subvisible particle analysis of biologics, Int. J. Pharm. 578 (2020), 119072.
[64] C. Probst, Characterization of Protein Aggregates, Silicone Oil Droplets, and Protein-Silicone Interactions Using Imaging Flow Cytometry, J. Pharm. Sci. 109 (2020) 364–374.
[65] H. Mach, A. Bhambhani, B.K. Meyer, S. Burek, H. Davis, J.T. Blue, R.K. Evans, The use of flow cytometry for the detection of subvisible particles in therapeutic protein formulations, J. Pharm. Sci. 100 (2011) 1671–1678.
[66] A.J. Paul, F. Bickel, M. Röhm, L. Hospach, B. Halder, N. Rettich, R. Handrick, E. M. Herold, H. Kiefer, F. Hesse, High-throughput analysis of sub-visible mAb

aggregate particles using automated fluorescence microscopy imaging, Anal. Bioanal. Chem. 409 (2017) 4149–4156.
[67] V. Filipe, A. Hawe, W. Jiskoot, Critical evaluation of Nanoparticle Tracking Analysis (NTA) by NanoSight for the measurement of nanoparticles and protein aggregates, Pharm. Res. 27 (2010) 796–810.
[68] V. Filipe, B. Kükrer, A. Hawe, W. Jiskoot, Transient molten globules and metastable aggregates induced by brief exposure of a monoclonal IgG to low pH, J. Pharm. Sci. 101 (2012) 2327–2339.
[69] D. Chen, S. Kapre, A. Goel, K. Suresh, S. Beri, J. Hickling, J. Jensen, M. Lal, J. Preaud, M. Laforce, Thermostable formulations of a hepatitis B vaccine and a meningitis A polysaccharide conjugate vaccine produced by a spray drying method, Vaccine 28 (2010) 5093–5099.
[70] J. Elversson, A. Millqvist-Fureby, Particle size and density in spray drying—effects of carbohydrate properties, J. Pharm. Sci. 94 (2005) 2049–2060.
[71] L. Chan, L. Tan, P.W. Heng, Process analytical technology: application to particle sizing in spray drying, Aaps Pharm. 9 (2008) 259–266.
[72] D. Vandenheuvel, A. Singh, K. Vandersteegen, J. Klumpp, R. Lavigne, G. Van den Mooter, Feasibility of spray drying bacteriophages into respirable powders to combat pulmonary bacterial infections, Eur. J. Pharm. Biopharm. 84 (2013) 578–582.
[73] P. Johansen, H.P. Merkle, B. Gander, Technological considerations related to the up-scaling of protein microencapsulation by spray-drying, Eur. J. Pharm. Biopharm. 50 (2000) 413–417.
[74] S.S. Kumar, C. Li, C.E. Christen, C.J. Hogan Jr, S.A. Fredericks, J. Hong, Automated droplet size distribution measurements using digital inline holography, J. Aerosol Sci. 137 (2019), 105442.
[75] M.U. Daloglu, A. Ray, M.J. Collazo, C. Brown, D. Tseng, B. Chocarro-Ruiz, L. M. Lechuga, D. Cascio, A. Ozcan, Low-cost and portable UV holographic microscope for high-contrast protein crystal imaging, APL Photonics 4 (2019), 030804.
[76] K. Dierks, A. Meyer, D. Oberthür, G. Rapp, H. Einspahr, C. Betzel, Efficient UV detection of protein crystals enabled by fluorescence excitation at wavelengths longer than 300 nm, Acta Crystallogr. Sect. F: Struct. Biol. Cryst. Commun. 66 (2010) 478–484.
[77] R.A. Judge, K. Swift, C. González, An ultraviolet fluorescence-based method for identifying and distinguishing protein crystals, Acta Crystallogr. D Biol. Crystallogr. 61 (2005) 60–66.
[78] K. Baumgartner, L. Galm, J. Nötzold, H. Sigloch, J. Morgenstern, K. Schleining, S. Suhm, S.A. Oelmeier, J. Hubbuch, Determination of protein phase diagrams by microbatch experiments: exploring the influence of precipitants and pH, Int. J. Pharm. 479 (2015) 28–40.
[79] I.M. Berry, O. Dym, R. Esnouf, K. Harlos, R. Meged, A. Perrakis, J. Sussman, T. Walter, J. Wilson, A. Messerschmidt, SPINE high-throughput crystallization, crystal imaging and recognition techniques: current state, performance analysis, new technologies and future aspects, Acta Crystallogr. D Biol. Crystallogr. 62 (2006) 1137–1149.
[80] A. Bohm, An inexpensive system for imaging the contents of multi-well plates, Acta Crystallogr. Sec. F Struct. Biol. Commun. 74 (2018) 797–802.
[81] A. Bohm, AMi: a GUI-based, open-source system for imaging samples in multi-well plates, Acta Crystallogr. Sec. F: Struct. Biol. Commun. 75 (2019) 531–536.
[82] C. Cumbaa, I. Jurisica, Automatic classification and pattern discovery in high-throughput protein crystallization trials, J. Struct. Funct. Genomics 6 (2005) 195–202.
[83] D. Handzlik, E.T. Larson, E. Munschy, G. Obmolova, D. Collin, T.K. Craig, Inexpensive robotic system for standard and fluorescent imaging of protein crystals, Acta Crystallogr. Sec. F Struct. Biol. Commun. 75 (2019) 673–686.
[84] M.E. Klijn, J. Hubbuch, Time-dependent multi-light-source image classification combined with automated multidimensional protein phase diagram construction for protein phase behavior analysis, J. Pharm. Sci. 109 (2020) 331–339.
[85] T. Lukk, R.E. Gillilan, D.M. Szebenyi, W.R. Zipfel, A visible-light-excited fluorescence method for imaging protein crystals without added dyes, J. Appl. Crystallogr. 49 (2016) 234–240.
[86] K. Mele, B.T. Lekamge, V.J. Fazio, J. Newman, Using time courses to enrich the information obtained from images of crystallization trials, Cryst. Growth Des. 14 (2014) 261–269.
[87] M. Sigdel, M.L. Pusey, R.S. Aygun, Crystpro: Spatiotemporal analysis of protein crystallization images, Cryst. Growth Des. 15 (2015) 5254–5262.
[88] C.Y. Ma, J.J. Liu, X.Z. Wang, Stereo imaging of crystal growth, AIChE J. 62 (2016) 18–25.
[89] E. Forsythe, A. Achari, M.L. Pusey, Trace fluorescent labeling for high-throughput crystallography, Acta Crystallogr. D Biol. Crystallogr. 62 (2006) 339–346.
[90] M. Pusey, E. Forsythe, A. Achari, Fluorescence approaches to growing macromolecule crystals, in Structural proteomics, Springer (2008) 377–385.
[91] H.S. Rho, H.-W. Veltkamp, A.T. Hanke, M. Ottens, C. Breukers, P. Habibović, H. Gardeniers, Systematic Investigation of Insulin Fibrillation on a Chip, Molecules 25 (2020) 1380.
[92] A. Shrestha, T. Tran, R. Aygun, M. Pusey, Mobile Scanner for Protein Crystallization Plates, in: 2018 IEEE International Symposium on Multimedia (ISM), IEEE, 2018, pp. 209-214.
[93] M. Sigdel, M.L. Pusey, R.S. Aygun, Real-time protein crystallization image acquisition and classification system, Cryst. Growth Des. 13 (2013) 2728–2736.
[94] C.L. Tarver, M. Pusey, A low-cost method for visible fluorescence imaging, Acta Crystallographica Section F: Structural Biology, Communications 73 (2017) 657–663.
[95] T. Tran, M. Pusey, R. Aygun, Mobile Fluorescence Imaging and Protein Crystal Recognition, in: 2020 IEEE 33rd International Symposium on Computer-Based Medical Systems (CBMS), IEEE, 2020, pp. 83-88.
[96] D. Watts, J. Müller-Dieckmann, G. Tsakanova, V.S. Lamzin, M.R. Groves, Quantitive evaluation of macromolecular crystallization experiments using 1, 8-ANS fluorescence, Acta Crystallogr. D Biol. Crystallogr. 66 (2010) 901–908.
[97] A. Echalier, R. Glazer, V. Fülöp, M. Geday, Assessing crystallization droplets using birefringence, Acta Crystallogr. D Biol. Crystallogr. 60 (2004) 696–702.
[98] P. Nollert, Microscope detection options for colorless protein crystals grown in lipidic cubic phases, J. Appl. Crystallogr. 36 (2003) 1295–1296.
[99] R.L. Owen, E. Garman, A new method for predetermining the diffraction quality of protein crystals: using SOAP as a selection tool, Acta Crystallogr. D Biol. Crystallogr. 61 (2005) 130–140.
[100] L.M. Haupert, G.J. Simpson, Screening of protein crystallization trials by second order nonlinear optical imaging of chiral crystals (SONICC), Methods 55 (2011) 379–386.
[101] D.J. Kissick, D. Wanapun, G.J. Simpson, Second-order nonlinear optical imaging of chiral crystals, Annu. Rev. Anal. Chem. 4 (2011) 419–437.
[102] R.D. Wampler, D.J. Kissick, C.J. Dehen, E.J. Gualtieri, J.L. Grey, H.-F. Wang, D. H. Thompson, J.-X. Cheng, G.J. Simpson, Selective detection of protein crystals by second harmonic microscopy, J. Am. Chem. Soc. 130 (2008) 14076–14077.
[103] K.A. Chan, L. Govada, R.M. Bill, N.E. Chayen, S.G. Kazarian, Attenuated total reflection-FT-IR spectroscopic imaging of protein crystallization, Anal. Chem. 81 (2009) 3769–3775.
[104] S.E. Glassford, L. Govada, N.E. Chayen, B. Byrne, S.G. Kazarian, Micro ATR FTIR imaging of hanging drop protein crystallisation, Vib. Spectrosc. 63 (2012) 492–498.
[105] M. Boulet-Audet, B. Byrne, S.G. Kazarian, High-throughput thermal stability analysis of a monoclonal antibody by attenuated total reflection FT-IR spectroscopic imaging, Anal. Chem. 86 (2014) 9786–9793.
[106] J. De Meutter, J. Vandenameele, A. Matagne, E. Goormaghtigh, Infrared imaging of high density protein arrays, Analyst 142 (2017) 1371–1380.
[107] H. Tiernan, B. Byrne, S.G. Kazarian, ATR-FTIR spectroscopy and spectroscopic imaging for the analysis of biopharmaceuticals, Spectrochim. Acta Part A Mol. Biomol. Spectros. (2020) 118636.
[108] H. Emteborg, R. Zeleny, J. Charoud-Got, G. Martos, J. Lüddeke, H. Schellin, K. Teipel, Infrared thermography for monitoring of freeze-drying processes: Instrumental developments and preliminary results, J. Pharm. Sci. 103 (2014) 2088–2097.
[109] E. Lietta, D. Colucci, G. Distefano, D. Fissore, On the use of infrared thermography for monitoring a vial freeze-drying process, J. Pharm. Sci. 108 (2019) 391–398.
[110] P.-J. Van Bockstal, J. Corver, L. De Meyer, C. Vervaet, T. De Beer, Thermal imaging as a noncontact inline process analytical tool for product temperature monitoring during continuous freeze-drying of unit doses, Anal. Chem. 90 (2018) 13591–13599.
[111] A. Ziaee, A.B. Albadarin, L. Padrela, T. Femmer, E. O'Reilly, G. Walker, Spray drying of pharmaceuticals and biopharmaceuticals: Critical parameters and experimental process optimization approaches, Eur. J. Pharm. Sci. 127 (2019) 300–318.
[112] D. Colucci, L. Morra, X. Zhang, D. Fissore, F. Lamberti, An automatic computer vision pipeline for the in-line monitoring of freeze-drying processes, Comput. Ind. 115 (2020), 103184.
[113] D. Colucci, J.M. Prats-Montalbán, A. Ferrer, D. Fissore, On-line product quality and process failure monitoring in freeze-drying of pharmaceutical products, Drying Technol. (2019) 1–14.
[114] D. Colucci, J.M. Prats-Montalbán, D. Fissore, A. Ferrer, Application of multivariate image analysis for on-line monitoring of a freeze-drying process for pharmaceutical products in vials, Chemometrics Intelligent Lab. Syst. 187 (2019) 19–27.
[115] G. Fabien, M.l. Antoni, K. Sefiane, Use of IR thermography to investigate heated droplet evaporation and contact line dynamics, Langmuir 27 (2011) 6744–6752.
[116] E. Wulsten, G. Lee, Surface temperature of acoustically levitated water microdroplets measured using infra-red thermography, Chem. Eng. Sci. 63 (2008) 5420–5424.
[117] E. Both, A. Karlina, R. Boom, M. Schutyser, Morphology development during sessile single droplet drying of mixed maltodextrin and whey protein solutions, Food Hydrocolloids 75 (2018) 202–210.
[118] J. Perdana, M.B. Fox, M.A. Schutyser, R.M. Boom, Single-droplet experimentation on spray drying: evaporation of a sessile droplet, Chem. Eng. Technol. 34 (2011) 1151–1158.
[119] J. Perdana, M.B. Fox, M.A. Schutyser, R.M. Boom, Mimicking spray drying by drying of single droplets deposited on a flat surface, Food Bioprocess Technol. 6 (2013) 964–977.
[120] D. Brouckaert, L. De Meyer, B. Vanbillemont, P.-J. Van Bockstal, J. Lammens, S.v. Mortier, J. Corver, C. Vervaet, I. Nopens, T. De Beer, Potential of near-infrared chemical imaging as process analytical technology tool for continuous freeze-drying, Analytical chemistry, 90 (2018) 4354-4362.
[121] H. Trnka, A. Palou, P.E. Panouillot, A. Kauppinen, M. Toiviainen, H. Grohganz, M. Alcalà, M. Juuti, J. Ketolainen, J. Rantanen, Near-infrared imaging for high-throughput screening of moisture induced changes in freeze-dried formulations, J. Pharm. Sci. 103 (2014) 2839–2846.
[122] R. de Souza Lima, A. Braeuer, P. Arlabosse, M.-I. Ré, In situ Raman composition profiling in drying droplets, Powder Technol. 373 (2020) 232–241.
[123] M. Nuzzo, J. Sloth, B. Brandner, B. Bergenstahl, A. Millqvist-Fureby, Confocal Raman microscopy for mapping phase segregation in individually dried particles composed of lactose and macromolecules, Colloids Surf., A 481 (2015) 229–236.

[124] J.P. Pajander, S. Matero, J. Sloth, F. Wan, J. Rantanen, M. Yang, Raman mapping of mannitol/lysozyme particles produced via spray drying and single droplet drying, Pharm. Res. 32 (2015) 1993–2002.
[125] T. Starciuc, Y. Guinet, L. Paccou, A. Hedoux, Influence of a small amount of glycerol on the trehalose bioprotective action analyzed in situ during freeze-drying of lyzozyme formulations by micro-Raman spectroscopy, J. Pharm. Sci. 106 (2017) 2988–2997.
[126] H. Trnka, J. Rantanen, H. Grohganz, Well-plate freeze-drying: a high throughput platform for screening of physical properties of freeze-dried formulations, Pharm. Dev. Technol. 20 (2015) 65–73.
[127] H. Trnka, J.X. Wu, M. Van De Weert, H. Grohganz, J. Rantanen, Fuzzy logic-based expert system for evaluating cake quality of freeze-dried formulations, J. Pharm. Sci. 102 (2013) 4364–4374.
[128] S. Gretzinger, S. Limbrunner, J. Hubbuch, Automated image processing as an analytical tool in cell cryopreservation for bioprocess development, Bioprocess Biosyst. Eng. 42 (2019) 665–675.
[129] M.E. Klijn, J. Hubbuch, Influence of image analysis strategy, cooling rate, and sample volume on apparent protein cloud-point temperature determination, Bioprocess and biosystems engineering, Accepted manuscript (2020).
[130] M.E. Klijn, A.K. Wöll, J. Hubbuch, Apparent protein cloud point temperature determination using a low volume high-throughput cryogenic device in combination with automated imaging, Bioprocess Biosyst. Eng. 43 (2020) 439–456.
[131] A.K. Wöll, M. Desombre, L. Enghauser, J. Hubbuch, A phase diagram-based toolbox to assess the impact of freeze/thaw ramps on the phase behavior of proteins, Bioprocess Biosyst. Eng. 43 (2020) 179–192.
[132] A.K. Wöll, J. Hubbuch, Investigation of the reversibility of freeze/thaw stress-induced protein instability using heat cycling as a function of different cryoprotectants, Bioprocess Biosyst. Eng. (2020) 1–19.
[133] A.K. Wöll, J. Schütz, J. Zabel, J. Hubbuch, Analysis of phase behavior and morphology during freeze-thaw applications of lysozyme, Int. J. Pharm. 555 (2019) 153–164.
[134] D. Colucci, D. Fissore, A.A. Barresi, R.D. Braatz, A new mathematical model for monitoring the temporal evolution of the ice crystal size distribution during freezing in pharmaceutical solutions, Eur. J. Pharm. Biopharm. 148 (2020) 148–159.
[135] D. Colucci, R. Maniaci, D. Fissore, Monitoring of the freezing stage in a freeze-drying process using IR thermography, Int. J. Pharm. 566 (2019) 488–499.
[136] U. Roessl, D. Jajcevic, S. Leitgeb, J.G. Khinast, B. Nidetzky, Characterization of a laboratory-scale container for freezing protein solutions with detailed evaluation of a freezing process simulation, J. Pharm. Sci. 103 (2014) 417–426.
[137] A. Hedoux, L. Paccou, S. Achir, Y. Guinet, Mechanism of protein stabilization by trehalose during freeze-drying analyzed by in situ micro-raman spectroscopy, J. Pharm. Sci. 102 (2013) 2484–2494.
[138] T. Starciuc, B. Malfait, F. Danede, L. Paccou, Y. Guinet, N.T. Correia, A. Hedoux, Trehalose or Sucrose: Which of the Two Should be Used for Stabilizing Proteins in the Solid State? A Dilemma Investigated by In Situ Micro-Raman and Dielectric Relaxation Spectroscopies During and After Freeze-Drying, J. Pharm. Sci. 109 (2020) 496–504.
[139] J. Pincemaille, A. Banc, E. Chauveau, J.-M. Fromental, L. Ramos, M.-H. Morel, P. Menut, Methods for screening cloud point temperatures, Food Biophys. 13 (2018) 422–431.
[140] P. Cheng, D. Li, L. Boruvka, Y. Rotenberg, A. Neumann, Automation of axisymmetric drop shape analysis for measurements of interfacial tensions and contact angles, Colloids Surf. 43 (1990) 151–167.
[141] F. Lin, D. Kwok, Z. Policova, W. Zingg, A. Neumann, The effect of ph and concentration on the surface tension of adsorbed layers of various insulin preparations, Colloids Surf., B 3 (1995) 281–286.
[142] Y. Rotenberg, L. Boruvka, A. Neumann, Determination of surface tension and contact angle from the shapes of axisymmetric fluid interfaces, J. Colloid Interface Sci. 93 (1983) 169–183.
[143] A. Voigt, O. Thiel, D. Williams, Z. Policova, W. Zingg, A. Neumann, Axisymmetric drop shape analysis (ADSA) applied to protein solutions, Colloids Surf. 58 (1991) 315–326.
[144] L. Yang, M. Biswas, P. Chen, Study of binding between protein A and immunoglobulin G using a surface tension probe, Biophys. J . 84 (2003) 509–522.
[145] ISO/FDIS 26924:2013. Particle characterization of particulate systems. Vocabulary., in.
[146] L.O. Narhi, J. Schmit, K. Bechtold-Peters, D. Sharma, Classification of protein aggregates, J. Pharm. Sci. 101 (2012) 493–498.
[147] A.S. Rosenberg, Effects of protein aggregates: an immunologic perspective, AAPS J. 8 (2006) E501–E507.
[148] J.G. Barnard, K. Babcock, J.F. Carpenter, Characterization and quantitation of aggregates and particles in interferon-β products: potential links between product quality attributes and immunogenicity, J. Pharm. Sci. 102 (2013) 915–928.
[149] C.F. Chisholm, B.H. Nguyen, K.R. Soucie, R.M. Torres, J.F. Carpenter, T. W. Randolph, In vivo analysis of the potency of silicone oil microdroplets as immunological adjuvants in protein formulations, J. Pharm. Sci. 104 (2015) 3681–3690.
[150] V. Corvari, L.O. Narhi, T.M. Spitznagel, N. Afonina, S. Cao, P. Cash, I. Cecchini, M. R. DeFelippis, P. Garidel, A. Herre, Subvisible (2–100 μm) particle analysis during biotherapeutic drug product development: Part 2, experience with the application of subvisible particle analysis, Biologicals 43 (2015) 457–473.
[151] S.K. Singh, N. Afonina, M. Awwad, K. Bechtold-Peters, J.T. Blue, D. Chou, M. Cromwell, H.J. Krause, H.C. Mahler, B.K. Meyer, An industry perspective on the monitoring of subvisible particles as a quality attribute for protein therapeutics, J. Pharm. Sci. 99 (2010) 3302–3321.
[152] V. Filipe, A. Hawe, J.F. Carpenter, W. Jiskoot, Analytical approaches to assess the degradation of therapeutic proteins, TrAC, Trends Anal. Chem. 49 (2013) 118–125.
[153] C.-T. Huang, D. Sharma, P. Oma, R. Krishnamurthy, Quantitation of protein particles in parenteral solutions using micro-flow imaging, J. Pharm. Sci. 98 (2009) 3058–3071.
[154] S. Cao, L. Narhi, Y. Jiang, R.S. Rajan, Analytical methods to measure subvisible particulates, in: Analysis of aggregates and particles in protein pharmaceuticals, Wiley Online Library, 2012, pp. 85-115.
[155] A. Hawe, D. Weinbuch, S. Zölls, A. Reichel, J.F. Carpenter, Submicrometer, micrometer and visible particle analysis in biopharmaceutical research and development, in: Biophysical Characterization of Proteins in Developing Biopharmaceuticals, Elsevier, 2020, pp. 285-310.
[156] H.-C. Mahler, W. Friess, U. Grauschopf, S. Kiese, Protein aggregation: pathways, induction factors and analysis, J. Pharm. Sci. 98 (2009) 2909–2934.
[157] A. Malloy, B. Carr, NanoParticle tracking analysis–The halo™ system, Part. Part. Syst. Char. 23 (2006) 197–204.
[158] X. Tian, M.R. Nejadnik, D. Baunsgaard, A. Henriksen, C. Rischel, W. Jiskoot, A comprehensive evaluation of nanoparticle tracking analysis (NanoSight) for characterization of proteinaceous submicron particles, J. Pharm. Sci. 105 (2016) 3366–3375.
[159] A.P. Defante, W.N. Vreeland, K.D. Benkstein, D.C. Ripple, Using image attributes to assure accurate particle size and count using nanoparticle tracking analysis, J. Pharm. Sci. 107 (2018) 1383–1391.
[160] F. Depreter, G. Pilcer, K. Amighi, Inhaled proteins: challenges and perspectives, Int. J. Pharm. 447 (2013) 251–280.
[161] P.C. Seville, H.-Y. Li, T.P. Learoyd, Spray-dried powders for pulmonary drug delivery, Critical Rev.™ Therapeutic Drug Carrier Systems 24 (2007).
[162] M. Bowen, R. Turok, Y.-F. Maa, Spray drying of monoclonal antibodies: investigating powder-based biologic drug substance bulk storage, Drying Technol. 31 (2013) 1441–1450.
[163] A. Ziaee, A.B. Albadarin, L. Padrela, M.-T. Ung, T. Femmer, G. Walker, E. O'Reilly, A rational approach towards spray drying of biopharmaceuticals: The case of lysozyme, Powder Technol. (2020).
[164] A.D. Brunaugh, T. Wu, S.R. Kanapuram, H.D. Smyth, Effect of Particle Formation Process on Characteristics and Aerosol Performance of Respirable Protein Powders, Mol. Pharm. 16 (2019) 4165–4180.
[165] R. Geidobler, G. Winter, Controlled ice nucleation in the field of freeze-drying: fundamentals and technology review, Eur. J. Pharm. Biopharm. 85 (2013) 214–222.
[166] C. Takeiti, T. Kieckbusch, F. Collares-Queiroz, Morphological and physicochemical characterization of commercial maltodextrins with different degrees of dextrose-equivalent, Int. J. Food Prop. 13 (2010) 411–425.
[167] J.A. Searles, J.F. Carpenter, T.W. Randolph, The ice nucleation temperature determines the primary drying rate of lyophilization for samples frozen on a temperature-controlled shelf, J. Pharm. Sci. 90 (2001) 860–871.
[168] M.J. Maltesen, S. Bjerregaard, L. Hovgaard, S. Havelund, M. Van De Weert, Quality by design–Spray drying of insulin intended for inhalation, Eur. J. Pharm. Biopharm. 70 (2008) 828–838.
[169] C. Sadek, P. Schuck, Y. Fallourd, N. Pradeau, C. Le Floch-Fouere, R. Jeantet, Drying of a single droplet to investigate process–structure–function relationships: a review, Dairy Sci. Technol. 95 (2015) 771–794.
[170] A. Arsiccio, A. Sparavigna, R. Pisano, A. Barresi, Measuring and predicting pore size distribution of freeze-dried solutions, Drying Technol. 37 (2019) 435–447.
[171] I. Russo Krauss, A. Merlino, A. Vergara, F. Sica, An overview of biological macromolecule crystallization, Int. J. Mol. Sci. 14 (2013) 11643–11691.
[172] N. Asherie, Protein crystallization and phase diagrams, Methods 34 (2004) 266–272.
[173] A. McPherson, Introduction to protein crystallization, Methods 34 (2004) 254–265.
[174] B. Rupp, Origin and use of crystallization phase diagrams, Acta Crystallographica Section F: Structural Biology, Communications 71 (2015) 247–260.
[175] A.C. Dumetz, A.M. Chockla, E.W. Kaler, A.M. Lenhoff, Protein phase behavior in aqueous solutions: crystallization, liquid-liquid phase separation, gels, and aggregates, Biophys. J . 94 (2008) 570–583.
[176] M.L. Pusey, R.S. Aygün, Data analytics for protein crystallization, Springer, 2017.
[177] J.R. Luft, J.R. Wolfley, E.H. Snell, What's in a drop? Correlating observations and outcomes to guide macromolecular crystallization experiments, Crystal Growth Des. 11 (2011) 651–663.
[178] J.P. Zeelen, Interpretation of the crystallization drop results, Protein Crystallization Techniques, Strategies, and Tips, TM Bergfors, Ed.(International University Line, CA, 1999), (2009) 131.
[179] C.A. Cumbaa, A. Lauricella, N. Fehrman, C. Veatch, R. Collins, J. Luft, G. DeTitta, I. Jurisica, Automatic classification of sub-microlitre protein-crystallization trials in 1536-well plates, Acta Crystallogr. D Biol. Crystallogr. 59 (2003) 1619–1627.
[180] S. Schorsch, J.-H. Hours, T. Vetter, M. Mazzotti, C.N. Jones, An optimization-based approach to extract faceted crystal shapes from stereoscopic images, Comput. Chem. Eng. 75 (2015) 171–183.
[181] S. Desbois, S.A. Seabrook, J. Newman, Some practical guidelines for UV imaging in the protein crystallization laboratory, Acta Crystallogr. Sec. F Struct. Biol. Crystallizat. Commun. 69 (2013) 201–208.
[182] M.L. Pusey, R.S. Aygün, Robotic image acquisition, in: Data Analytics for Protein Crystallization, Springer, 2017, pp. 57-81.

[183] A.E. Bruno, P. Charbonneau, J. Newman, E.H. Snell, D.R. So, V. Vanhoucke, C. J. Watkins, S. Williams, J. Wilson, Classification of crystallization outcomes using deep convolutional neural networks, PLoS ONE 13 (2018), e0198883.
[184] T.X. Tran, M.L. Pusey, R.S. Aygun, Protein Crystallization Segmentation and Classification Using Subordinate Color Channel in Fluorescence Microscopy Images, J. Fluorescence (2020) 1–20.
[185] C.A. Cumbaa, I. Jurisica, Protein crystallization analysis on the world community grid, J. Struct. Funct. Genomics 11 (2010) 61–69.
[186] K. Saitoh, K. Kawabata, H. Asama, T. Mishima, M. Sugahara, M. Miyano, Evaluation of protein crystallization states based on texture information derived from greyscale images, Acta Crystallogr. D Biol. Crystallogr. 61 (2005) 873–880.
[187] J.T. Ng, C. Dekker, M. Kroemer, M. Osborne, F. von Delft, Using textons to rank crystallization droplets by the likely presence of crystals, Acta Crystallogr. D Biol. Crystallogr. 70 (2014) 2702–2718.
[188] J.T. Madden, E.L. DeWalt, G.J. Simpson, Two-photon excited UV fluorescence for protein crystal detection, Acta Crystallogr. D Biol. Crystallogr. 67 (2011) 839–846.
[189] P. Padayatti, G. Palczewska, W. Sun, K. Palczewski, D. Salom, Imaging of protein crystals with two-photon microscopy, Biochemistry 51 (2012) 1625–1637.
[190] S. Buchala, J.C. Wilson, Improved classification of crystallization images using data fusion and multiple classifiers, Acta Crystallogr. D Biol. Crystallogr. 64 (2008) 823–833.
[191] P.T. Ingvarsson, S.T. Schmidt, D. Christensen, N.B. Larsen, W.L.J. Hinrichs, P. Andersen, J. Rantanen, H.M. Nielsen, M. Yang, C. Foged, Designing CAF-adjuvanted dry powder vaccines: spray drying preserves the adjuvant activity of CAF01, J. Control. Release 167 (2013) 256–264.
[192] M.J. Maltesen, M. Van De Weert, Drying methods for protein pharmaceuticals, Drug Discovery Today: Technologies 5 (2008) e81–e88.
[193] J. Massant, S. Fleurime, M. Batens, H. Vanhaerents, G. Van den Mooter, Formulating monoclonal antibodies as powders for reconstitution at high concentration using spray-drying: Trehalose/amino acid combinations as reconstitution time reducing and stability improving formulations, Eur. J. Pharm. Biopharm. 156 (2020) 131–142.
[194] A. Pfützner, T. Forst, Pulmonary insulin delivery by means of the Technosphere™ drug carrier mechanism, Expert Opin. Drug Delivery 2 (2005) 1097–1106.
[195] D.C. Geraldes, V.L. Beraldo-de-Araújo, B.O.P. Pardo, A. Pessoa Junior, M. A. Stephano, L. de Oliveira-Nascimento, Protein drug delivery: current dosage form profile and formulation strategies, J. Drug Target. 28 (2020) 339–355.
[196] W. Wang, Lyophilization and development of solid protein pharmaceuticals, Int. J. Pharm. 203 (2000) 1–60.
[197] A. Langford, B. Bhatnagar, R. Walters, S. Tchessalov, S. Ohtake, Drying of biopharmaceuticals: Recent developments, new technologies and future direction, Japan J. Food Eng. 19 (2018) 15–24.
[198] K. Cal, K. Sollohub, Spray drying technique. I: Hardware and process parameters, J. Pharm. Sci. 99 (2010) 575–586.
[199] A.M. Abdul-Fattah, D.S. Kalonia, M.J. Pikal, The challenge of drying method selection for protein pharmaceuticals: product quality implications, J. Pharm. Sci. 96 (2007) 1886–1916.
[200] Y.-F. Maa, P.-A. Nguyen, T. Sweeney, S.J. Shire, C.C. Hsu, Protein inhalation powders: spray drying vs spray freeze drying, Pharm. Res. 16 (1999) 249–254.
[201] M. Ameri, Y.-F. Maa, Spray drying of biopharmaceuticals: stability and process considerations, Drying Technol. 24 (2006) 763–768.
[202] S. Nail, S. Tchessalov, E. Shalaev, A. Ganguly, E. Renzi, F. Dimarco, L. Wegiel, S. Ferris, W. Kessler, M. Pikal, Recommended best practices for process monitoring instrumentation in pharmaceutical freeze drying—2017, Aaps Pharmscitech 18 (2017) 2379–2393.
[203] J.A.W.M. Corver, Method and system for freeze-drying injectable compositions, in particular pharmaceutical compositions, in, Google Patents (2018).
[204] B. Adhikari, T. Howes, B. Bhandari, V. Truong, Experimental studies and kinetics of single drop drying and their relevance in drying of sugar-rich foods: A review, Int. J. Food Prop. 3 (2000) 323–351.
[205] N. Fu, M.W. Woo, X.D. Chen, Single droplet drying technique to study drying kinetics measurement and particle functionality: A review, Drying Technol. 30 (2012) 1771–1785.
[206] M.A. Schutyser, J. Perdana, R.M. Boom, Single droplet drying for optimal spray drying of enzymes and probiotics, Trends Food Sci. Technol. 27 (2012) 73–82.
[207] E. Breen, J. Curley, D. Overcashier, C. Hsu, S. Shire, Effect of moisture on the stability of a lyophilized humanized monoclonal antibody formulation, Pharm. Res. 18 (2001) 1345–1353.
[208] J.K. Towns, Moisture content in proteins: its effects and measurement, J. Chromatogr. A 705 (1995) 115–127.
[209] M.J. Pikal, S. Shah, Intravial distribution of moisture during the secondary drying stage of freeze drying, PDA J. Pharm. Sci. Technol. 51 (1997) 17–24.
[210] K. Fischer, Neues Verfahren zur maßanalytischen Bestimmung des Wassergehaltes von Flüssigkeiten und festen Körpern, Angew. Chem. 48 (1935) 394–396.
[211] P. Matejtschuk, C. Duru, K. Malik, E. Ezeajughi, E. Gray, S. Raut, F. Mawas, Use of thermogravimetric analysis for moisture determination in difficult lyophilized biological samples, American J. Analyt. Chem. 7 (2016) 260.
[212] M.S. Kamat, R.A. Lodder, P.P. DeLuca, Near-infrared spectroscopic determination of residual moisture in lyophilized sucrose through intact glass vials, Pharm. Res. 6 (1989) 961–965.
[213] A. Kauppinen, M. Toiviainen, O. Korhonen, J. Aaltonen, K. Järvinen, J. Paaso, M. Juuti, J. Ketolainen, In-line multipoint near-infrared spectroscopy for moisture content quantification during freeze-drying, Anal. Chem. 85 (2013) 2377–2384.
[214] U.S.F.D. Administation, Lyophilization of Parenterals (7/39), in: Guide to inspections of lyophilization of parenterals, 2014.
[215] S.M. Patel, S.L. Nail, M.J. Pikal, R. Geidobler, G. Winter, A. Hawe, J. Davagnino, S.R. Gupta, Lyophilized drug product cake appearance: what is acceptable? J. Pharm. Sci. 106 (2017) 1706–1721.
[216] C. Haeuser, P. Goldbach, J. Huwyler, W. Friess, A. Allmendinger, Imaging techniques to characterize cake appearance of freeze-dried products, J. Pharm. Sci. 107 (2018) 2810–2822.
[217] R. Pisano, A.A. Barresi, L.C. Capozzi, G. Novajra, I. Oddone, C. Vitale-Brovarone, Characterization of the mass transfer of lyophilized products based on X-ray micro-computed tomography images, Drying Technol. 35 (2017) 933–938.
[218] P.L. Privalov, Cold denaturation of protein, Crit. Rev. Biochem. Mol. Biol. 25 (1990) 281–306.
[219] G.B. Strambini, E. Gabellieri, Proteins in frozen solutions: evidence of ice-induced partial unfolding, Biophys. J . 70 (1996) 971–976.
[220] P. Sundaramurthi, R. Suryanarayanan, The effect of crystallizing and non-crystallizing cosolutes on succinate buffer crystallization and the consequent pH shift in frozen solutions, Pharm. Res. 28 (2011) 374–385.
[221] A. Hottot, S. Vessot, J. Andrieu, Freeze drying of pharmaceuticals in vials: Influence of freezing protocol and sample configuration on ice morphology and freeze-dried cake texture, Chem. Eng. Process. Process Intensif. 46 (2007) 666–674.
[222] D.S. Goldberg, S.M. Bishop, A.U. Shah, H.A. Sathish, Formulation development of therapeutic monoclonal antibodies using high-throughput fluorescence and static light scattering techniques: role of conformational and colloidal stability, J. Pharm. Sci. 100 (2011) 1306–1315.
[223] J.C. Gimel, D. Durand, T. Nicolai, Structure and distribution of aggregates formed after heat-induced denaturation of globular proteins, Macromolecules 27 (1994) 583–589.
[224] V. Militello, C. Casarino, A. Emanuele, A. Giostra, F. Pullara, M. Leone, Aggregation kinetics of bovine serum albumin studied by FTIR spectroscopy and light scattering, Biophys. Chem. 107 (2004) 175–187.
[225] F. Vollrath, N. Hawkins, D. Porter, C. Holland, M. Boulet-Audet, Differential Scanning Fluorimetry provides high throughput data on silk protein transitions, Sci. Rep. 4 (2014) 5625.
[226] N. Sreerama, R.W. Woody, Computation and analysis of protein circular dichroism spectra, in: Methods in enzymology, Elsevier, 2004, pp. 318-351.
[227] R.W. Williams, [14] Protein secondary structure analysis using Raman amide I and amide III spectra, in: Methods in enzymology, Elsevier, 1986, pp. 311-331.
[228] J.L.R. Arrondo, A. Muga, J. Castresana, F.M. Goñi, Quantitative studies of the structure of proteins in solution by Fourier-transform infrared spectroscopy, Prog. Biophys. Mol. Biol. 59 (1993) 23–56.
[229] K.A. Chan, S.G. Kazarian, High-throughput study of poly (ethylene glycol)/ibuprofen formulations under controlled environment using FTIR imaging, J. Comb. Chem. 8 (2006) 26–31.
[230] S.G. Kazarian, K.A. Chan, ATR-FTIR spectroscopic imaging: recent advances and applications to biological systems, Analyst 138 (2013) 1940–1951.
[231] G. Serin, H.H. Nguyen, J.-D. Marty, J.-C. Micheau, V.r. Gernigon, A.-F.o. Mingotaud, D. Bajon, T. Soulet, S.b. Massenot, C. Coudret, Terahertz time-domain spectroscopy of thermoresponsive polymers in aqueous solution, The Journal of Physical Chemistry B, 120 (2016) 9778-9787.
[232] N. Penkov, V. Yashin, E. Fesenko Jr, A. Manokhin, E. Fesenko, A study of the effect of a protein on the structure of water in solution using terahertz time-domain spectroscopy, Appl. Spectrosc. 72 (2018) 257–267.
[233] C. Cao, Z. Zhang, X. Zhao, T. Zhang, Terahertz spectroscopy and machine learning algorithm for non-destructive evaluation of protein conformation, Opt. Quant. Electron. 52 (2020) 1–18.
[234] Z. Zang, S. Yan, X. Han, D. Wei, H.-L. Cui, C. Du, Temperature-and pH-dependent protein conformational changes investigated by terahertz dielectric spectroscopy, Infrared Phys. Technol. 98 (2019) 260–265.
[235] M.L. Broide, T.M. Tominc, M.D. Saxowsky, Using phase transitions to investigate the effect of salts on protein interactions, Phys. Rev. E 53 (1996) 6325.
[236] D.N. Petsev, X. Wu, O. Galkin, P.G. Vekilov, Thermodynamic functions of concentrated protein solutions from phase equilibria, J. Phys. Chem. B 107 (2003) 3921–3926.
[237] O. Galkin, P.G. Vekilov, Control of protein crystal nucleation around the metastable liquid–liquid phase boundary, Proc. Natl. Acad. Sci. 97 (2000) 6277–6281.
[238] E.J. Park, Y.C. Bae, Cloud-point temperatures of lysozyme in electrolyte solutions by thermooptical analysis technique, Biophys. Chem. 109 (2004) 169–188.
[239] A. Boire, P. Menut, M.-H. Morel, C. Sanchez, Phase behaviour of a wheat protein isolate, Soft Matter 9 (2013) 11417–11426.
[240] A.S. Raut, D.S. Kalonia, Pharmaceutical perspective on opalescence and liquid–liquid phase separation in protein solutions, Mol. Pharm. 13 (2016) 1431–1444.
[241] J. Bloustine, T. Virmani, G. Thurston, S. Fraden, Light scattering and phase behavior of lysozyme-poly (ethylene glycol) mixtures, Phys. Rev. Lett. 96 (2006), 087803.
[242] J. Grigsby, H. Blanch, J. Prausnitz, Cloud-point temperatures for lysozyme in electrolyte solutions: effect of salt type, salt concentration and pH, Biophys. Chem. 91 (2001) 231–243.
[243] C. Ishimoto, T. Tanaka, Critical behavior of a binary mixture of protein and salt water, Phys. Rev. Lett. 39 (1977) 474.
[244] M. Muschol, F. Rosenberger, Liquid–liquid phase separation in supersaturated lysozyme solutions and associated precipitate formation/crystallization, J. Chem. Phys. 107 (1997) 1953–1962.
[245] W. Wang, C.J. Roberts, Protein aggregation–mechanisms, detection, and control, Int. J. Pharm. 550 (2018) 251–268.

[246] S. Amrhein, K.C. Bauer, L. Galm, J. Hubbuch, Non-invasive high throughput approach for protein hydrophobicity determination based on surface tension, Biotechnol. Bioeng. 112 (2015) 2485–2494.
[247] E. Keshavarz, S. Nakai, The relationship between hydrophobicity and interfacial tension of proteins, Biochimica et Biophysica Acta (BBA)-Protein, Structure 576 (1979) 269–279.
[248] A.I. Rusanov, V.A. Prokhorov, Interfacial tensiometry, Elsevier Science B.V, Amsterdam, 1996.
[249] D.B. Thiessen, Surface tension measurement, CRC Handbook Chem. Phys. (1999).
[250] Y. Zuo, A. Neumann, Application of axisymmetric drop shape analysis (ADSA) to the study of biomolecules, in: Molecular Interfacial Phenomena of Polymers and Biopolymers, Elsevier, 2005, pp. 249-285.
[251] M. Molony, C. Undey, PAT tools for biologics: Considerations and challenges, in: Quality by Design for Biopharmaceuticals: Principles and Case Studies, John Wiley & Sons, 2011.
[252] G. Reich, Near-infrared spectroscopy and imaging: basic principles and pharmaceutical applications, Adv. Drug Deliv. Rev. 57 (2005) 1109–1143.